

**Alma Mater Studiorum – Università di Bologna**

**DOTTORATO DI RICERCA IN**

**Biologia Cellulare, Molecolare e Industriale:  
Biologia Funzionale dei Sistemi Cellulari e  
Molecolari**

**Ciclo XXIV**

Settore Concorsuale di afferenza: 05/E2

Settore Scientifico disciplinare: BIO-11

PhD thesis:

***Characterization of the structure and iron uptake  
mechanisms of the Staphylococcus aureus ferric  
hydroxamate-binding lipoprotein FhuD2***

Presentata da: **Mariotti Paolo**

**Coordinatore Dottorato**

**Prof. Scarlato Vincenzo**

**Relatore**

**Dott. Bagnoli Fabio**

**Prof. Scarlato Vincenzo**

**Esame finale anno 2012**

**~ 1 ~**



# CONTENTS

ABSTRACT .....	7
INTRODUCTION .....	9
<i>Reverse vaccinology overview</i> .....	9
<i>Structural Vaccinology</i> .....	11
<i>Staphylococcus aureus</i> .....	12
<i>Staphylococcus aureus iron uptake molecular mechanisms</i> .....	14
<i>The staphylococcus aureus ferric hydroxamate-binding lipoprotein FhuD2</i> .....	17
AIM OF THE WORK .....	22
METHODS .....	23
<i>Cloning and protein expression</i> .....	23
<i>Circular dichroism</i> .....	26
<i>Differential Scanning Fluorescence, (DSF)</i> .....	28
<i>Surface Plasmon Resonance (SPR)</i> .....	29
<i>Crystallization, data collection, and structure solution</i> .....	31
RESULTS .....	33
<i>FhuD2<sub>(18-302)</sub> and FhuD2<sub>(27-302)</sub> constructs retain the major overall structural elements</i> .....	33
<i>DSF thermal denaturation experiments and circular dichroism analysis</i> .....	35
<i>Structural studies of FhuD2</i> .....	37

<i>A network of polar and hydrophobic interactions form the groove where FhuD<sub>27-302</sub> captures ferrichrome</i> .....	48
<i>Interaction between transferrin and iron-free ferrichrome</i> .....	54
DISCUSSION.....	56
REFERENCES: .....	68





# ABSTRACT

Extraordinary advancements in the use of vaccines have been made in the last decades. Approaches and developments in this area of medicine considering the work of scientists from Edward Jenner and Louis Pasteur until Jonas Salk and Albert Sabin are impressive, but now, their traditional technologies have been largely out-dated by important innovations in the field. Traditional technologies for vaccine development are totally tied to a work flow that requires the identification of the factors important for immunity by using a fixed approach that begins with the cultivation of the pathogenic microorganism and ends up with a functional characterization by using biochemical, immunological and microbiological methodologies. The Reverse Vaccinology (RV) approach, at present, brings the new possibility to use genomic information for the delineation of new protein-based vaccines starting from an *in silico* analysis. The first powerful example of the application of the RV approach is given by the development of a protein-based vaccine against serogroup B *Meningococcus*. A similar approach was also used to identify new *Staphylococcus aureus* vaccine candidates, including the ferric hydroxamate-binding lipoprotein FhuD2. *S. aureus* is a widespread human pathogen, which employs various different strategies for iron uptake, including: (i) siderophore-mediated iron acquisition using the endogenous siderophores staphyloferrin A and B, (ii) siderophore-mediated iron acquisition using xeno-siderophores (the pathway exploited by FhuD2) and (iii) heme-mediated iron acquisition. In this work the high resolution crystal structure of FhuD2 in the iron

(III)-siderophore-bound form was determined. FhuD2 belongs to the Periplasmic Binding Protein family (PBP ) class III, and is principally formed by two globular domains, at the N- and C-termini of the protein, that make up a cleft where ferrichrome-iron (III) is bound. The N- and C-terminal domains, connected by a single long  $\alpha$ -helix, present Rossmann-like folds, showing a  $\beta$ -stranded core and an  $\alpha$ -helical periphery, which do not undergo extensive structural rearrangement when they interact with the ligand, typical of class III PBP members. The structure shows that ferrichrome-bound iron does not come directly into contact with the protein; rather, the metal ion is fully coordinated by six oxygen donors of the hydroxamate groups of three ornithine residues, which, with the three glycine residues, make up the peptide backbone of ferrichrome. Furthermore, it was found that iron-free ferrichrome is able to subtract iron from transferrin. This study shows for the first time the structure of FhuD2, which was found to bind to siderophores ,and that the protein plays an important role in *S. aureus* colonization and infection phases.



# INTRODUCTION

## *Reverse Vaccinology overview*

Genomics tools and the exponentially growing number of bacterial genome sequencing projects have changed the landscape of modern biology providing a new opportunity of vaccine development. Conceptually, a project that involves the use of RV could be summarized by the following essential concepts: (i) surface exposure of antigens is a critical and essential requisite for the immune response interaction to pathogens; (ii) similarity of primary sequence to proteins associated with virulence or immunogenicity is a parameter of selection for the antigen; (iii) finally, to formulate a protective vaccine it is important to take into account the conservation of the chosen antigen within different pathogens and serotypes, knowing that many bacterial pathogens adopt the strategy of gene variability to escape the immune system. In addition, RV can be used associated with systematic transcriptomic and proteomic gene expression analysis, helping the identification of gene-level responses, which are correlated with protection *in vivo* and then facilitating the rational design of a hypothetical vaccine candidate [1]. All pathogens, for which vaccines are not yet available, as well as parasites and viruses could be subjected to this new concept of vaccine design. It is commonly known that, to escape from immune response some pathogens are able to adopt a mechanism of sequence variability; however some antigens are sufficiently

conserved in subpopulations that have not undergone this defense mechanism, therefore it is important to select them for the development of broadly protective vaccines [2], [3], [4]. Another aspect that RV takes into consideration is the integration (iv) with proteomic and transcriptomic gene expression data. In fact proteomic and DNA microarray analysis could be used to investigate when and to what extent antigens are expressed *in vitro* and *in vivo* during infection. A protein whose expression is limited to part of an organism's life-cycle that is irrelevant to human carriage or invasive disease, may be immunogenic and surface expressed but of little use as a vaccine [5]; alternatively, a protein expressed transiently at a stage of the life-cycle, critical for the process of invasion, may be an ideal target for a vaccine. Also, in order to avoid either poor immunogenicity or autoimmunity, vaccine candidates have to be selected without any sequence similarity (v) with human proteins.

## *Structural Vaccinology*

Approximately 50,000 high-resolution protein structures are available in public databases (the PDB, protein data bank), and several initiatives have been established to pursue high-throughput characterization of protein structures on a genome-wide scale [6]. The study of structural properties of protein antigens has opened the new field of Structural Vaccinology [7], where the ability to predict the immunogenic potential of an antigen is considered the first challenge of vaccinology. Structural biology has demonstrated that antibodies usually recognize conformational epitopes which can not be predicted by sequence analysis. Several studies have shown that protective epitopes can be identified by structural studies of antigen–antibody complexes [8]; [9]; [10]. Also, the identification and characterization of many basic principles of proteins, nucleic acid structures, molecular machines and viruses have become possible in the past few decades using structural biology studies. Therefore, structural vaccinomics appears to have a large range of possible applications in the biomedical field and it is easy to understand why structure-based development of therapeutics is already linked to the pharmaceutical industry simply observing how this fundamental tool is necessary for the identification of important drugs directed at the active sites of enzymes [11], such as the inhibitors for HIV-1 protease [12] and influenza virus neuraminidase [13]. Several advances that have facilitated the rational design of a vaccine, driving the birth and growth of structural vaccinomics, include high-throughput robotic crystallization systems, cryo-crystallography, high energy synchrotrons, structure phasing approaches using anomalous signal, [14] have made structural vaccinology

one of the most important tools to understand the relationships between immunological epitopes and tertiary structure of proteins [15]. From this more “structural” point of view it is possible to aid the optimization of vaccine antigens by genetic engineering, predict conformational epitopes, increase conformational stability and the breadth of protection, improve the safety profile, and therefore eliminate non-protective immunodominant epitopes [16], [9], [17], [18], [19], [15]. An example of how a structure-based approach has been already used in vaccine design is provided by an NMR spectroscopy study used to obtain the structure in solution of the immunodominant domain of GNA1870, a protective antigen of *N. meningitidis* identified by reverse vaccinology. The epitopes of bactericidal antibodies against several meningococcal strain variants were mapped onto the NMR structure of GNA1870, providing the basis for the rational design of an engineered form of 1870 containing several cross-protective, high affinity B cell epitopes [20]; [21].

### ***Staphylococcus aureus***

Bacteria in the genus *Staphylococcus* are opportunistic pathogens of humans, mammals and other vertebrates, and commonly invade the host when its immunodefenses are lowered. They grow in clusters, pairs, and occasionally, short chains. These specific clusters arise because staphylococci divide in two planes. The structural configuration of the *cocci* is a critical parameter to distinguish *micrococci* and *staphylococci* from *streptococci*, which grow in chains [22]. The catalase test is considered a useful criterion to distinguish staphylococci from streptococci and

other Gram-positive *cocci*, which are catalase negative. Staphylococci are Gram-positive non-motile *cocci*, usually 1µm in diameter, traditionally divided into two groups based on their ability to clot blood (the coagulase reaction). The coagulase-positive staphylococci form the species *S. aureus*; it may infect any organ, normally causing a little, focal lesion (e.g. a boil or a sty) and can also originate bacteremia, septicemia, deep-wound infections, endocarditis, pneumonia, and/or osteomyelitis [23]; [24]; [25]. *S. aureus* is able to express toxins and enzymes that contribute to pathogenicity and is also involved in the scalded skin syndrome and the toxic shock syndrome. From 1999 to 2005, the estimated number of US *S. aureus*-related hospitalizations increased 62%, approximately 295,000 to 480,000 cases. Also, the estimated number of methicillin-resistant *Staphylococcus aureus* (MRSA) related hospitalizations more than doubled, from approximately 127,000 to 278,000 (US), [26] in the same time frame. In fact *S. aureus* easily develops resistance to antibiotics, thus presenting an important clinical challenge. MRSA infections are of increasing importance to clinicians, public health agencies and governments. Community associated methicillin-resistant *S. aureus* (CA-MRSA) has also become a major problem in US hospitals already dealing with high levels of hospital-associated MRSA (HA-MRSA): in outpatients, the frequency of CA-MRSA isolates has increased more than sevenfold during 1999–2006 [27]. Therefore, research strategies must be addressed to understand better the processes that promote *S. aureus* pathogenesis, as they could represent important targets for novel therapeutics.

## ***Staphylococcus aureus iron uptake molecular mechanisms***

Transition metals are essential nutrients to all forms of life, including bacterial pathogens. Iron is one of the major factors necessary for growth. It is a critical nutrient for both humans and pathogenic bacteria, and most organisms require iron as an essential element in a variety of metabolic and cellular pathways. In humans, iron-containing compounds are involved in several important cellular processes including energy metabolism, cellular proliferation, DNA repair, and protection against oxidative stress [28],[29],[30]. In *S. aureus*, iron also participates in processes such as metabolism and DNA synthesis, and is a determinant for regulation of virulence factors, defense against oxidative stress and therefore essential for bacterial pathogenesis. To prevent bacterial infection, the human immune system has developed a particular feature that provides the capture of iron as a form of innate immune response against bacterial infection. This human defense mechanism [31] (nutritional immunity) provides that a host sequesters nutrients essential to bacterial growth by (i) decreasing dietary iron absorption, (ii) reducing release of iron from macrophages, and (iii) releasing of apo-lactoferrin from neutrophil granules at the site of infection [32]; thus limiting the ability of invading pathogens to proliferate in the host environment. Iron is then maintained predominantly intracellularly or in complex with high-affinity host binding proteins [32] maintaining an extracellular iron concentration insufficient for bacterial growth [33]. Consequently, staphylococci have counter-evolved different systems for iron-uptake, based on the ability of processing and stealing iron from iron-containing host molecules or proteins. During infection, *S. aureus* is able to bypass nutritional

immunity and obtain iron from the host (*e.g.*, from Heme, or transferrin) with different mechanisms. *S. aureus*, uses hemolysins that lyse red blood cells to cause the release of hemoglobin, which can be further degraded to heme and free iron. In response to infections, as previously reported, the host fortifies iron sequestration and free iron is bound by transferrin and lactoferrin, free heme by hemopexin, and hemoglobin by haptoglobin to limit iron availability to invading pathogens [34].

To circumvent iron-limiting host defenses *S. aureus* produces two polycarboxylate-type siderophores, which can bind iron with very high affinity: staphyloferrin A, which is a 479 Da molecule encoded by the *sfaABCD* gene cluster [35], [36], and staphyloferrin B, a 448 Da compound composed of L-2,3-diaminopropionic acid, 1,2-diaminoethane, and  $\alpha$ -ketoglutaric acid produced by the *sbnABCDEFGHI* operon, (only *SbnC*, *SbnE*, *SbnF*, and *SbnH* are required for in vitro synthesis) [37]. Bacterial Staphyloferrin A and Staphyloferrin B establish a competition on iron sequestration with host lactoferrin and transferrin. Import into the pathogen of iron bound to staphyloferrin A and staphyloferrin B is then mediated by *HtsABC* and *SirABC*, respectively, in processes powered by the *FhuC* ATPase. Iron acquisition by staphyloferrin A and staphyloferrin B is regulated by the ferric uptake regulator (*Fur*) in response to environmental iron concentrations [35],[38],[39]. *Fur* is an iron-dependent transcriptional regulator that is conserved among Gram-positive and Gram-negative bacteria [40]. When a sufficiently high concentration of iron is present, *Fur* binds a consensus DNA sequence (*Fur* box) upstream of *Fur*-regulated genes, leading to transcriptional repression. In iron-depleted conditions, *Fur* no longer binds to *Fur* boxes, and transcription of *Fur*-regulated genes can proceed. In this way, *S. aureus* can initiate a transcriptional program based on the amount of iron available in the environment [41]. Another mechanism involved in iron uptake

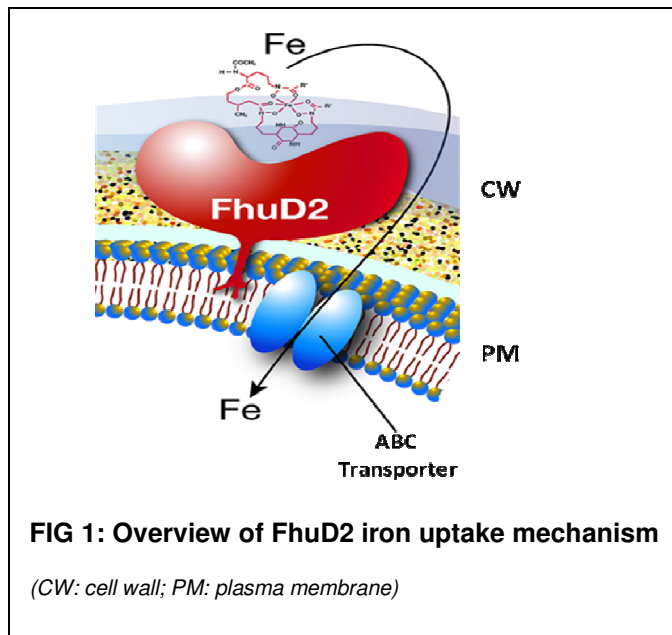
is the Isd system that mediates acquisition of iron from heme, which is the preferred iron source during *S. aureus* infections [42]. Bacterial heme acquisition systems involve cell surface receptors that recognize either free heme or heme bound to hemoproteins, a transport apparatus to move heme across the cell membrane into the bacterial cytoplasm, and enzymes that liberate iron from heme [43]. Specifically in *S. aureus*, IsdB and IsdH are cell-surface receptors for hemoglobin and hemoglobin-haptoglobin, respectively. IsdB and IsdH pass heme to IsdA, or alternatively to IsdC or IsdE, culminating in transport across the cell membrane by IsdDEF. In the cytoplasm, heme is degraded by IsdG or IsdI to release iron [44], [42].



## *The Staphylococcus aureus ferric hydroxamate-binding lipoprotein*

### *FhuD2*

*S. aureus* presents two general mechanisms for iron uptake. One includes systems that are able to acquire heme from hemoglobin and transfer it through the cell wall to a membrane-localized transporter system (Isd pathway) and to final degradation once into the cell [45]. The second mechanism is based on utilizing siderophores for scavenging iron and transfer the siderophore-iron complex inside the cell for further processing and iron extraction. To show more in details how siderophores complexed with iron collected from the environment are “prey” of specific high affinity receptors, it necessary to introduce the concept that there are two classes of siderophore: (i) endogenous siderophore, expressed by *S. aureus*, as Staphyloferrin A and Stafiloferrin B or (ii) Xeno-siderophore, that are siderophore expressed from other bacteria, but able to participate in the *S. aureus* iron uptake mechanisms [46]. The second case involves hydroxamate xeno-siderophores as ferrichrome, coprogen, aerobactin and desferrioxamine B, that are able to establish interactions with *S. aureus* ferric hydroxamate-binding lipoprotein FhuD2 [47]; [48]; which is currently known to use only xeno-sideophores. FhuD2 is encoded in an operon, which contains three genes, fhuCBG, encoding a heterodimeric receptor coupled to a classical ATPase, while a fourth and a fifth gene, (fhuD2 and fhuD1, respectively) encoding for two lipoproteins necessary for the binding of iron and its transfer into the cell, drive the iron ferric-hydroxamate uptake pathway [49]. fhuD1 is predicted to encode a protein with approximately 50% amino acid sequence identity to FhuD2 [47]. FhuD2 is a lipoprotein able to bind iron-siderophore complexes and mediates



acquisition of iron via the dedicated ABC transporter (FhuCBG). Sequence analyses reveal that the closely related *S. aureus* paralogs FhuD2 and FhuD1 are orthologs of several siderophore-binding proteins of other bacteria, with

examples including the Gram-positive *B. subtilis* FhuD lipoprotein, and the Gram-negative *E. coli* periplasmic proteins FhuD, FepB, FecB and BtuF [45]. These proteins show sequence identities with FhuD2 ranging from 15-35%, and they all belong to the large family of Binding Proteins, which share an overall architecture presenting a ligand-binding groove between two globular domains each containing a central  $\beta$ -sheet surrounded by  $\alpha$ -helices.

FhuD2 belongs to this large protein family, initially known as the Periplasmic Binding Proteins family, which became known more simply as Binding Proteins upon the discovery that the family encompasses surface lipoproteins of Gram-positive bacteria [50, 51]. The Binding Protein family shares an overall architecture of a ligand-binding groove located between two distinct globular domains each containing a central  $\beta$ -sheet surrounded by  $\alpha$ -helices.

This family of proteins has the capacity of binding a wide range of solutes, including oxyanions, amino acids, peptides, carbohydrates and siderophores, and of shuttling these ligands to membrane-bound receptors that mediate active transport into the cytoplasm, providing the range of nutrients essential for bacterial survival

and growth [50, 51]. In a structure-based manner, this family has been sub-divided into three main classes, depending largely on the nature of the linker(s) connecting the two globular domains [51, 52].

The class I proteins, including the prototypical maltose-binding protein (MBP), have three short connecting segments or hinges, usually  $\beta$ -strands, between the two domains. In contrast, the class II proteins have two crossovers, while the class III proteins only have one segment connecting the two domains. For the class I and II proteins, the ligand is fully engulfed; the binding induces a notable structural change: a hinge motion of 20-30° in the flexible inter-domain connector, bringing the two globular domains closer together, in what has been termed a ‘Venus fly-trap’ mechanism [53]. The latter is exemplified by MBP [54, 55], and leucine-binding protein (LBP)[56], structures of which have been determined in the apo and ligand-bound states. The closed, ligand-bound conformation engages the membrane-bound receptor, thus initiating substrate transport, uptake, or chemotaxis. In contrast, FhuD2 and close relatives belong to class III, wherein a single long  $\alpha$ -helix connects the two globular domains and is thought to impose a structural rigidity that prevents large inter-domain rearrangements [50].

Recently, class III has been further sub-divided into FhuD-like or TroA-like Binding Proteins families, mainly due to minor differences in composition of the  $\beta$ -sheets central to each lobe and the length of the  $\alpha$ -helix connecting the lobes [50]. In structural studies of apo- and ligand-bound forms of the *E. coli* proteins FhuD [57-59] and BtuF [60], the long  $\alpha$ -helix appears to prevent Venus fly-trap-like domain rearrangements, suggesting an alternative mechanism governing receptor engagement and substrate transport which may involve direct recognition of both parts of the protein-ligand complex [61]. Herein we focus on the FhuD-like Binding

Proteins family, since we are less concerned with the uptake of transition metal ions by the TroA-like sub-class [62] but rather with iron acquisition in pathogenic bacteria, which is required for infection and survival in host tissues [63, 64] and therefore important in vaccine design. FhuD2 was first identified as part of the ferric hydroxamate uptake (fhu) system [65] that regulates uptake of iron (III) siderophores [49, 66-68]. There are ~500 known siderophores secreted by bacteria, yeasts, fungi and plants; they are low molecular weight organic chelators with very high and specific affinity for iron (III) and they function to mediate iron uptake by microbial cells. Siderophores can be classified in hydroxamate, catecholate or hydroxycarboxylate siderophores, depending on the functional groups used for iron coordination [69]. In *S. aureus*, FhuD2 mediates hydroxamate siderophore import via a dedicated ATP-binding cassette (ABC) transporter – the receptor complex FhuCBG, in which FhuB and FhuG form the transmembrane transporter, dependent on the ATPase activity of the cytoplasmic sub-unit FhuC. Among these siderophores, FhuD2 is dedicated to the uptake of iron (III) hydroxamate siderophores [65]. As such, FhuD2 was quickly recognized as having a potentially important role in supporting the basic physiological processes of *S. aureus*, since free iron is very poorly available in the host environment [69]. Indeed, FhuD2 is part of an extensive set of mechanisms that *S. aureus* employs for obtaining iron, including direct acquisition via the heme group of hemoglobin (the Isd pathway) or alternative approaches based on siderophores that scavenge extracellular iron and allow uptake of iron-siderophore complexes. The latter can be bound by Staphylococcal Binding Proteins such as HtsA and SirA, which recognize the endogenous staphyloferrin A and staphyloferrin B (both  $\alpha$ -hydroxycarboxylate-type siderophores), [70] and [66], respectively. In contrast, FhuD2 appears to bind

exclusively to hydroxamate xeno-siderophores, including ferrichrome, coprogen, aerobactin and desferal [71], and the FhuCBG complex then mediates ATP-dependent transport across the Staphylococcal membrane. Although several members of the family have been studied previously, comprehensive studies of FhuD2 and its mechanism of ligand binding have not been reported to date.

Comparative genomic analysis shows that the *fhuD2* gene belongs to the core genome of *S. aureus* and is very well conserved across epidemiologically relevant strains (R. Mishra et al. 2012). Protection efficacy of FhuD2 was evaluated using kidney abscess and sepsis mouse models (R. Mishra et al. 2012). A marked reduction in bacterial count in kidney of immunized mice was coupled with diminished number and size of abscesses as compared to control. In the sepsis model, significant increase of survival was recorded after immunization with FhuD2. Protection was also obtained by passive immunization and sera raised against FhuD2 were shown to mediate opsonophagocytosis of staphylococcal cells in in vitro assays. In addition, FhuD2 plays a critical role in *S. aureus* virulence in mouse infection models. Collectively, these data suggest that FhuD2 represents a promising vaccine candidate against *S. aureus* (R. Mishra et al. 2012).

# AIM OF THE WORK

This study was designed to characterize molecular interactions of hydroxamate siderophores with the *S. aureus* lipoprotein FhuD2 and determine its X-ray crystal structure. Finally, the role of FhuD2 in subtracting iron from host blood proteins and in staphylococcal virulence was investigated. Overall, these studies are expected to provide crucial information for the understanding of FhuD2-mediated iron acquisition mechanisms during staphylococcal infective processes.

# METHODS

## *Cloning and Protein Expression*

We designed several protein construct based on the primary structure of *S. aureus* strain NCTC8325 FhuD2 that shows 302 AA including a predicted N-terminal secretion signal and a Cys lipidation target at position 18. All the ORFs were cloned using pET24b+, pET21b+, petTEV or pMKsal plasmids and two of these (Fig 2) have been engineered also using DISOPRED2 (<http://bioinf.cs.ucl.ac.uk/disopred/>), Jpred, (<http://www.compbio.dundee.ac.uk/www-jpred/>) disorder prediction server, and SER, Surface Entropy Reduction server (<http://services.mbi.ucla.edu/SER/>). These servers, based on a library of 800 non redundant high resolution protein structures, have indicated a high degree of disorder in the N terminal part of FhuD2 and a short region composed of three aminoacids (Lys 94, Glu 95 and Lys 96) with high surface entropy level. Therefore we have designed FhuD2<sub>27-302</sub> consisting of residues 27-302, and FhuD2 3aaa, consisting of residues 27-302 accommodating three point mutations, specifically K94A E95A K96A. All produced constructs have been verified by DNA sequencing, expressed in *Escherichia coli* BL21(DE3) and grown in LB or HTMC medium at 27 or 30°C for 8 or 30 h, respectively. Protein expression has been inducted by addition of 4 mM IPTG when optical density reached 0.8 at 600 nm. Only *E. coli* containing pMKsal did not receive IPTG

induction, since the plasmid presents an auto-induction growth mechanism. *E. coli* cells expressing the tagless recombinant FhuD2 constructs were resuspended in 50 mM Tris-HCl (pH 7.0) and disrupted in a French press apparatus (SLM Aminco, Rochester, N.Y.). After centrifugation at 30,000 x g, the supernatants of the transformed *E. coli* extracts were filtered through 0.22 µm membrane (Corning filter system). The lysate was then diluted with bidistilled water to adjust conductivity to 1.8-1.9 mS/cm and pH adjusted to 7.0. Soluble cell extract was then loaded onto SP Sepharose FF cation exchange resin (GE Healthcare) and protein eluted with a salt gradient from 0 to 1M NaCl, in 50 mM Na Phosphate pH 7.0 buffer. The relevant fractions have been selected by SDS-PAGE analysis (Criterion Bio-Rad) and the pool has been loaded on a Hydroxyapatite Ceramic Type I, 40µm (Bio-Rad) column equilibrated in 10 mM Phosphate pH 7.0 and eluted with a Na phosphate gradient from 10 mM to 500 mM, pH 7.0. The pool of fractions containing FhuD2, have been loaded on a preparative gel filtration column (Superdex 75, 26/60, GE Healthcare) and isocratically eluted in 20 mM Tris, 150 mM NaCl, 0.5 mM TCEP pH 8.0 buffer. The final pool was collected according to SDS PAGE analysis, then filtered on 0.22 µm membrane and concentrated to ~15 mg/ml for crystallization trials. Purity has been determined on RP-HPLC, ACE-300 C4 column, 4.6x300 mM in a 2 to 80% acetonitrile gradient in 0.1% TFA and purity confirmed to be >95%. Integrity has been determined on SE-HPLC, Tosoh TSG G3000SWxl column in phosphate buffer saline, and both constructs eluted at the expected MW (~30 KDa). Stability and contaminants controls were performed and will be described subsequently. Instead, *E. coli* cells expressing tag-recombinant FhuD2 were resuspended in 50 mM Tris-HCl (pH 8.0) and broken using Avestin Emulflex C-5 (14,000-15,000 psi) or sonicator (Branson Sonifier



450). After centrifugation at 16,000 x g (45 min), the supernatants of the pET-transformed *E. coli* extracts were filtered (Sartobran 300, 0,22 $\mu$ m) loaded onto nickel-activated chelating Sepharose columns (GE Healthcare His-trap HP), and after column washing with buffer containing 20 mM imidazole, recombinant proteins were eluted with 250 mM imidazole buffer elution. The protein concentration was determined with Bradford (Bio-Rad, Protein Assay) and BCA (Pierce) assays, using BSA as standard reference. In some case or in case of doubt the final protein concentration was determined by UV absorbance assuming  $E_{1\%, 1\text{cm}, 280\text{nm}} = 17.07$ . For determination of the protein purity and identity by Western Blot analysis the SDS-PAGE gel was blotted on nitro-cellulose membrane by I-Blot System (Invitrogen). For *E.coli* contaminants determination,  $\alpha$ -*E.coli* antibody (Dako) was used at 1:1000 dilution. For FhuD2 identity an  $\alpha$ -FhuD2 antibody (Rabbit 3) was used at 1:20000 dilution. The secondary-Antibody  $\alpha$ -Rabbit IgG horseradish peroxidase conjugated (Dako) was used at 1:10000 dilution and the membrane was developed with 4-chloro-naftol (Bio-Rad). Purity was also determined by Reverse Phase Chromatography, RP-HPLC, (Column: Vydac Protein C4, Cat. 214TP54. 4,6 ID x 250 mm, 5 mm.; Flow: 1 ml/min.; Injection: 50  $\mu$ l; in a 2 to 80% acetonitrile gradient in 0.1% TFA. MW was measured with SEC-HPLC analysis (Superdex 200 PC 3.2/30; Flow: 0.1 ml/min; Injection: 25  $\mu$ l; Buffer: PBS 1X; Method: isocratic conditions for 1.5 CV). The FhuD2 stability studies were performed at four different temperatures: -20°C, 4°C, Room Temperature (RT,  $\pm 25^\circ\text{C}$ ) and 37°C. The “state” of the protein was monitored with SDS-PAGE, SEC-HPLC and RP-HPLC for four weeks, by taking a sample each week. After purification and dialysis (vs. PBS) glycerol (30% vol/vol) was added as a cryo-protectant for storage at -80°C.

## ***Circular dichroism***

Circular dichroism (CD) is an excellent tool for determination of the secondary structure and folding properties of proteins that have been obtained using recombinant techniques or purified from tissues [72]. In most cases this application is inserted in a control process to determine whether a protein shows a specific folding, but also to check whether a mutation can cause changes in conformation or stability. In addition, it can be used to study protein interactions [73]. Circular dichroism relies on the differential absorption of left and right circularly polarized radiation by chromophores which either possess intrinsic chirality or are placed in chiral environments [74]. Proteins possess a number of chromophores which can give rise to CD signals. In the far UV region (240-180 nm), which corresponds to peptide bond absorption, the CD spectrum can be analyzed to give the content of regular secondary structural features such as  $\alpha$ -helix and  $\beta$ -sheet [74]. The CD spectrum in the near UV region (320-200 nm) reflects the environments of the aromatic amino acid side chains and thus gives information about the tertiary structure of the protein. Other non-protein chromophores such as flavin and haem moieties can give rise to CD signals which depend on the precise environment of the chromophore concerned [74]. In the protein design field, CD is used to assess the structure and stability of the designed protein fragments or their ligand binding, especially important in characterizing molten globule intermediates which may be involved in the folding process [74]. CD is an extremely useful technique for assessing the structural integrity of membrane proteins during extraction and characterization procedures. The interactions between chromophores can give rise to characteristic CD signals. This is well illustrated by the case of the light

harvesting complex from photosynthetic bacteria, where the CD spectra can be analyzed to indicate the extent of orbital overlap between the rings of bacteriochlorophyll molecules. It is therefore evident that CD is a versatile technique in structural biology, with an increasingly wide range of applications [74]. Far-UV CD spectra were recorded from 190 to 200 nm at 25°C using a Jasco-810 spectropolarimeter. The cuvette chamber was thermostated using a PerkinElmer PCB-1500 Peltier temperature system controller. Protein samples were at 0.1 mg/ml concentration in  $\text{KH}_2\text{NaPO}_4$  pH 7.2. A quartz cuvette with an optical path length of 1 mm was used. Spectra were acquired at 1 nm bandwidth, 0.5 sec response time, 0.2 nm step size and 10 nm/min scan speed. Each spectrum was calculated as the average of 5 accumulations. The results were corrected by subtracting the buffer baseline.

## *Differential Scanning Fluorescence, DSF*

Niesen , Berglund and Vedadi clearly show the importance of this tool for the choice of specific protein-ligand complexes to increase the probability to obtain crystals forms [75]. Differential scanning fluorimetry (DSF) is a rapid and inexpensive screening method to identify low-molecular-weight ligands that bind and stabilize purified proteins. The temperature at which a protein unfolds is measured by an increase in the fluorescence of a dye with affinity for hydrophobic parts of the protein, which are exposed as the protein unfolds [75]. A simple fitting procedure allows quick calculation of the transition midpoint. From the thermal unfolding curve, the midpoint of unfolding transition ( $T_m$ ) can be obtained and used to determine whether the protein is stabilized (increased  $T_m$ ) or destabilized (decreased  $T_m$ ) relative to a reference condition [76]. The difference in the temperature of this midpoint in the presence and absence of ligand is related to the binding affinity of the small molecule, which can be a low-molecular-weight compound, a peptide or a nucleic acid. DSF is best performed using a conventional real-time PCR instrument [75],[77]. Ligand solutions from a storage plate are added to a solution of protein and dye, distributed into the wells of the PCR plate and fluorescence intensity measured as the temperature is raised gradually [75]. A typical experiment was performed using a 96-well thin-wall PCR plate (Axigen). Both FhuD2<sub>18-302</sub>, FhuD2<sub>27-302</sub> and transferrin proteins were used at the final concentration of 6  $\mu$ M and the ferrichrome with or without iron at 18  $\mu$ M, for 1:3 as the final ratio for FhuD2 or 1:5 for transferrin. The SYPRO orange dye 5000X (Invitrogen), diluted 1:10 in 10 mM  $\text{KH}_2\text{PO}_4$ , pH 7.2, was utilized at the final concentration of 5X in each well. The final volume of reaction mixtures were 40  $\mu$ l

in 10 mM KH<sub>2</sub>PO<sub>4</sub>, pH 7.2. Fluorescence intensities were monitored in Stratagene Mx3005 RT-PCR instruments using the FAM (492 nm) and ROX (610 nm) filters for excitation and emission, respectively. Samples were heated from 25 °C to 95°C at scan rate of 1 °C/min. T<sub>m</sub> values were extrapolated fitting the raw data to Boltzmann model by GraphPad Prism 5.0 software.

### ***Surface plasmon resonance (SPR)***

Surface plasmon resonance (SPR) is a phenomenon that occurs in thin conducting films placed at the interface between two media of different refractive indices. In Biacore systems, a 50-nm layer of gold on the sensor chip is sandwiched between the glass layer of a sensor chip and the sample solution flowing through the microfluidic cartridge. Plane polarized light from a near-infrared LED is focused on the back of the sensor chip under conditions of total internal reflection and a diode array detector monitors the intensity of the reflected light [78],[79]. Under these conditions, the light leaks an electromagnetic component called an evanescent wave across the gold interface into the sample/buffer solution. At a certain angle of incident light, the evanescent wave field excites electrons in the gold film resulting in the formation of surface plasmons (electron charge density waves) within the gold film with a concomitant drop in the intensity of the reflected light at this angle (SPR angle). When a change in mass occurs near the sensor chip surface, e.g., as a result of a binding event, the angle of light at which SPR occurs shifts due to a change in refractive index near the sensor chip surface [79]. A sensorgram depicts

changes in SPR angle in real time, with responses measured in resonance units (RU). One RU corresponds to  $0.0001^\circ$  shift in SPR angle. SPR was used to monitor real-time interactions between protein and ligand, allowing direct measurement of the affinity constants. All SPR experiments were performed using a Biacore T100 (GE Healthcare) equilibrated at  $25^\circ\text{C}$ . FhuD2<sub>18-302</sub> and FhuD2<sub>27-302</sub> proteins were immobilized on the sensor surface and siderophores were injected in running buffer. For each titration, FhuD2(s) were first covalently immobilized by amine-coupling on a carboxymethylated dextran sensor chip (CM-5, GE Healthcare). Amine-coupling reactions for immobilization of FhuD2<sub>18-302</sub> and FhuD2<sub>27-302</sub> were performed using purified protein at  $\sim 10\mu\text{g/mL}$  in 10mM sodium acetate buffer pH 5 injected at  $5\mu\text{l/min}$  until  $\sim 3700$  response units (RU) were captured. A not modified surface was used as reference. Titration experiments were performed by injecting at  $20\mu\text{l/min}$  siderophores diluted in running buffer (filtered and degassed) containing Phosphate Buffered Saline (PBS) with 0.05% Tween-20 pH 7.4, to final concentrations ranging from 1nM to  $1\mu\text{M}$ . Following each injection, sensor chip surfaces were regenerated with a 45-second injection of 10mM Glycine pH 2.2. Each titration series contained 10-12 analyte injections. Data were analysed using the *BIAevaluation* software; a blank injection of buffer only was subtracted from each curve and reference sensorgrams were subtracted from experimental sensorgrams to yield curves representing specific binding. The shape of the curves prevented fitting the sensorgrams with any BIAevaluation kinetic models. Therefore long contact times (1050 s) were applied and steady-state analysis was used to plot equilibrium binding response ( $R_{\text{eq}}$ ) against analyte concentration in order to obtain the dissociation constants ( $K_{\text{D}}$ ).

### ***Crystallization, data collection, and structure solution***

Crystals of FhuD<sub>27-302</sub> complexed with ferrichrome were grown at 20°C by the vapor diffusion method. Crystallization experiments were prepared using 96-well low-profile Greiner crystallization plates in a nanodroplet sitting drop vapour diffusion format with 480 conditions screened at both 4°C and 20°C. Prior to crystallization, FhuD<sub>27-302</sub> at 20 mg/ml was incubated for 1 hour with a 5-fold molar excess of ferrichrome in a buffer containing 50mM Tris pH 8.0, 150mM NaCl, and 0.5mM TCEP. Crystals were grown in sitting drops prepared by mixing equal volumes (0.25µL) of the complex and of a reservoir solution consisting of 20% PEG-2000, 0.01M NiCl<sub>2</sub>, 0.1M Tris-HCl pH 8.5. All crystals were mounted using 20% ethylene glycol as a cryo-protectant prior to cooling to 100K for data collection.

Diffraction data were collected on beamline 5.0.3 of the Advanced Light Source (Lawrence Berkeley National Laboratory, Berkeley, CA, USA) and were processed using HKL2000 [80] and the CCP4 suite of programs [81]. The structure of FhuD<sub>27-302</sub> was solved by molecular replacement using Phaser [82], using as search model the coordinates of Protein Data Bank (PDB) entry for the *B. subtilis* FhuD-like protein BSU3320 (3G9Q). The final model was refined using Phenix [83] and Coot [84]. Model analysis was performed using Molprobity [85], and figures were generated with PyMOL (<http://www.pymol.org>). The geometry of the structure was excellent and all residues fell in allowed regions of the Ramachandran plot (Table 1). Crystals of FhuD<sub>27-302</sub> bound to ferrichrome belonged to space group P2<sub>1</sub>. The solution in both the rotation and translation functions indicated the

presence of one molecule in the asymmetric unit, which contained one FhuD<sub>27-302</sub> monomer bound to one molecule of ferrichrome, with a solvent content of 46% (Matthews coefficient 2.3 Å<sup>3</sup>/Da). Residues that differed between FhuD<sub>27-302</sub> and the search model were manually rebuilt using Coot with reference to 2Fo-Fc and Fo-Fc electron-density maps.



# RESULTS

## *FhuD2<sub>18-302</sub> and FhuD2<sub>27-302</sub> constructs retain the major overall structural elements*

Primary structure of FhuD2 shows a predicted N-terminal secretion signal, and a Cys lipidation target at position 18. DISOPRED2 disorder prediction server, based on a library of 800 non redundant and high resolution protein structures, has indicated a high degree of disorder in the N terminal part of FhuD2. Therefore, we have designed construct FhuD2<sub>18-302</sub>, consisting of residues 18-302 which correspond to the mature form of FhuD2, and construct FhuD2<sub>27-302</sub> consisting of residues 27-302 of FhuD2, in which the predicted “disordered” region (aa 18-26) was removed. On SE-HPLC elution times are identical for both forms (Fig 3). Peaks elute at an apparent MW of about 32 KDa consistent with their theoretical MW of 33 KDa. Integrity of the proteins is thus maintained, and no degradation products appeared on the chromatograms.

Also, from SDS PAGE (data not shown) the two constructs present identical migration profiles. Finally, both proteins, FhuD2<sub>18-302</sub> and FhuD2<sub>27-302</sub>, have the same circular dichroism profiles (Fig 3, panel B). In fact circular dichroism spectroscopy of both FhuD2 samples revealed that they shared the same, predominantly  $\alpha$ -helical secondary structure content.



**FIG 2:** Sequence of FhuD2<sub>18-302</sub> and FhuD2<sub>27-302</sub> constructs

These experiments taken together indicate that the predicted disordered amino-acids stretch at N-terminus did not affect the overall protein structure and could therefore be removed.

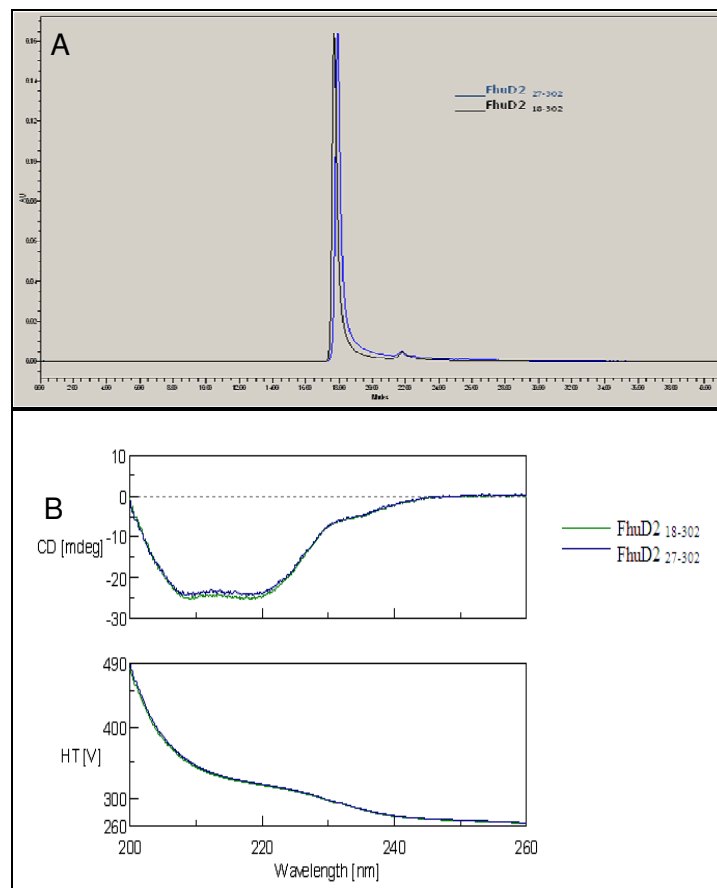


**FIG 3:** Analytical size-exclusion chromatography elution profiles of FhuD2<sub>18-302</sub> and FhuD2<sub>27-302</sub> (panel A); Far-UV CD spectra of FhuD2<sub>18-302</sub> and FhuD2<sub>27-302</sub> show the double-minima around 208nm and 220nm, typical of  $\alpha$ -helical secondary structure elements (panel B)

## ***DSF thermal denaturation experiments and Circular Dichroism analysis***

To test stability and functional integrity of the purified FhuD2 samples DSF thermal denaturation experiments were performed by heating FhuD2<sub>18-302</sub> and FhuD2<sub>27-302</sub>, in presence and in absence of ferrichrome in a 1:3 protein to siderophore ratio, from 25°C to 95°C. In the absence of ferrichrome, FhuD2<sub>18-302</sub> and FhuD2<sub>27-302</sub> had the same  $T_m$  value of 51.6 °C. However, the presence of ferrichrome induced an increment of  $T_m$  for both proteins of about 15.5°C, indicating that the both proteins in the presence of ferrichrome assume a more stable folding.

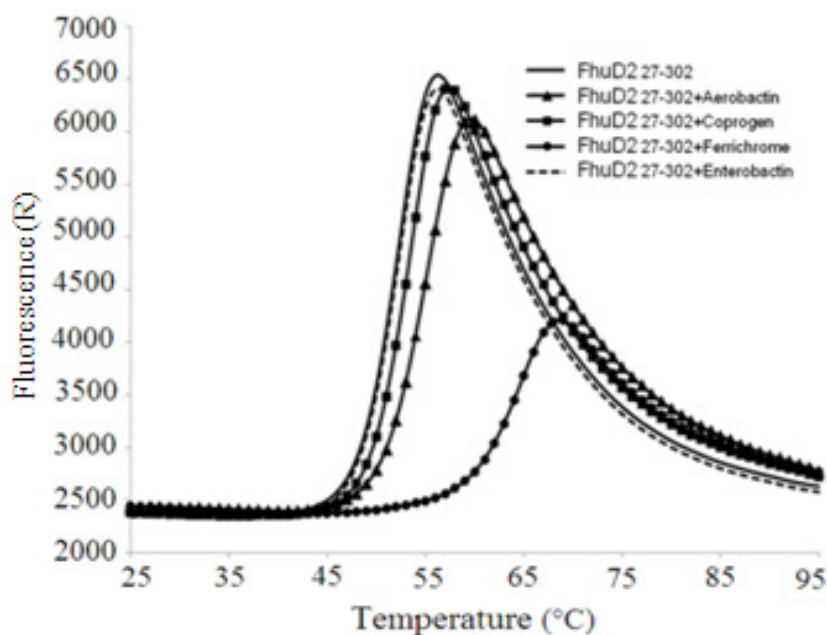


**FIG 4:** Differential scanning fluorimetry (DSF) reveals that iron (III) hydroxamate siderophores increase the thermal stability of FhuD2. The addition of iron-loaded ferrichrome to both FhuD2 constructs increases the  $T_m$  (identified as the first inflection point on the melting curve) from 51.6°C to 66.1°C, demonstrating thermal stabilization of the protein. The overall reduction in fluorescence intensity upon addition of ferrichrome is due to a quenching effect of Fe<sup>3+</sup>-ferrichrome on the fluorescent dye used in the DSF assay.

The lower observed fluorescence intensities in the presence of ferrichrome is due to a quenching effect of the Fe (III) on the dye fluorescence emission. In addition, in order to characterize the specificity of different families of siderophores, thermal denaturation was induced by heating FhuD<sub>27-302</sub> from 25°C to 95°C, in the presence of various hydroxamate siderophores, (aerobactin, coprogen and ferrichrome), and a catecolate siderophore (enterobactin) or without siderophore as negative control (Fig 4).

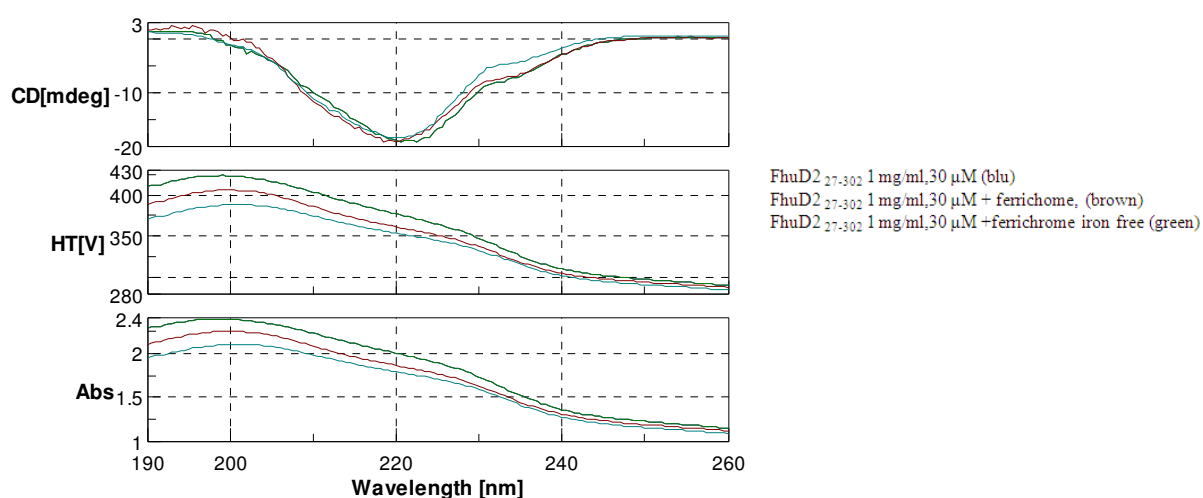


**FIG4A:** Circular dichroism analysis with FhuD<sub>27-302</sub> and ferrichrome with and without iron bound

All siderophores have been added in a 1:3 protein to siderophore final ratio. FhuD<sub>27-302</sub> has shown the highest  $T_m$  increase in the presence of ferrichrome, ( $\Delta T_m +15,5^\circ\text{C}$ ) compared to the other siderophores tested. Aerobactin and coprogen did not induce significant  $T_m$  increase ( $\Delta T_m +3^\circ\text{C}$  and  $\Delta T_m +1^\circ\text{C}$ , respectively). As expected catecholic siderophore enterobactin did not induce any stabilizing effect to FhuD<sub>27-302</sub>, showing identical  $T_m$  to the apo-protein. We also tested if the interaction with ferrichrome could be cause of a considerable structural

rearrangement of FhuD<sub>27-302</sub>, measurable with the CD analysis. As possible to observe in Fig 4A, CD analysis did not show any significant secondary structure rearrangement in the presence or absence of ferrichrome bound to the protein.

### *Structural studies of FhuD2*

In sitting drop experiment 0.25  $\mu$ l of a 50 mM Tris, 150 mM NaCl, 0.5 mM TCEP, pH 8.0 solution containing FhuD<sub>27-302</sub> 20 mg/ml and ferrichrome in a protein to siderophore molar ratio of 1 : 5 added to 0.25  $\mu$ l reservoir well solution (20% PEG-2000, 0.01 M NiCl<sub>2</sub>, 0.1 M TRIS pH 8.5) after five days gave rise to visible crystalline structures (Fig 5).

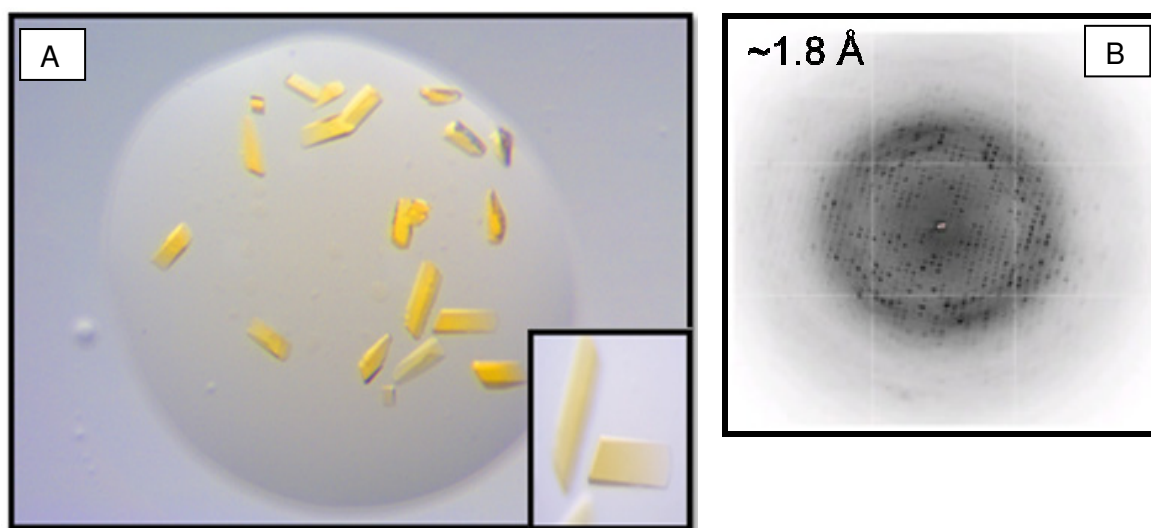
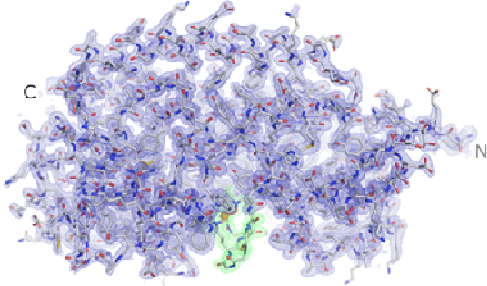


**FIG 5:** Crystals forms of FhuD<sub>27-302</sub> bound with ferrichrome (20% PEG-2000, 0.01 M NiCl<sub>2</sub>, 0.1 M TRIS pH 8.5) (Panel A); High resolution diffraction pattern of FhuD<sub>27-302</sub> crystals (Panel B)

All obtained crystals were mounted using 20% ethylene glycol as a cryo-protectant prior to cooling to 100K for data collection. Diffraction data were collected on beamline 5.0.3 at the Advanced Light Source facility (Lawrence Berkeley National Laboratory, Berkeley, CA, USA) (Fig 5, panel B). The structure of holo-FhuD<sub>27-302</sub> was solved employing a crystal of FhuD<sub>27-302</sub> which diffracted at 1.8 Å and molecular replacement with a homologous known structure from *B. subtilis* as an initial search model (FhuD, SEQID 38% [Protein Data Bank (PDB) code: 3G9Q], using the program PHASER [82]. The solution in both the rotation and translation functions (Tab 1) indicated the presence of one molecule in the asymmetrical unit, which was also suggested by the Matthews coefficient and solvent content [86]. Residues that differed between FhuD<sub>27-302</sub> and the search model were manually rebuilt using the program Coot [84] under the guidance of Fo2Fc and 2Fo2Fc electron-density maps. The structure of the 33 kDa holo- FhuD<sub>27-302</sub> in complex with its ligand ferrichrome (FeIII) was solved by molecular replacement and refined against 1.8 Å diffraction data to a R factors of 19% and Rfree 23.2%, respectively (Tab 1). All crystals used to obtain the structure belonged to the P<sub>2</sub><sub>1</sub> space group.

Structural analysis of collected data showed that overall folding (represented as a cartoon in Fig 6), of holo-FhuD<sub>27-302</sub> consists of two globular domains linked by one alpha helix. N-lobe, in green, consists of 121 amino acids, C-lobe, in blue, of 129 amino acids and the long alpha helix, in pink, of approximately 25 amino acids. The N-terminal lobe exhibits a central four-stranded parallel β-sheet surrounded by six short α-helices and flanked by a pair of additional, N-terminal, anti-parallel β-strands. The C-terminal lobe has a five main stranded mixed β-sheet surrounded by five α-helices and four short helical turns. The protein has an approximate dimensions of 60 Å x 40 Å x 35 Å and the siderophore-receptor site lies in a

shallow groove  $\sim 17\text{\AA}$  deep between the N-terminal and C-terminal cuts across the narrowest dimension of the protein.



Data collection	
Space group	$P 2_1$
Cell dimensions	
a, b, c (Å)	53.8, 50.1, 54.3
$\alpha, \beta, \gamma$ (°)	90, 106.4, 90
Resolution (Å)	43.3–1.8
$R_{\text{sym}}$ or $R_{\text{merge}}$	10.5 (31.7)
$I/\sigma I$	5.6 (1.0)
Completeness (%)	99.9 (99.9)
Redundancy	5.6 (3.6)
Refinement	
Resolution (Å)	43.3–1.8
No. reflections	25,928
$R_{\text{work}}$ / $R_{\text{free}}}$	19/23.2
No. atoms	
Protein	2155
Ligand/ion	75
Water	145
B-factors	
Protein	30.4
Ligand/ion	35.8
Water	37.1
R.m.s deviations	
Bond lengths (Å)	0.014
Bond angles (°)	0.999
Ramachandran	
Most favoured	91.4%
Additional allowed	8.6%
Generously allowed	0.0%
Disallowed	0.0%

\*Highest resolution shell is shown in parenthesis.  
 $R_{\text{sym}} = \sum_k \sum_l \sum_h |I(hkl) - \langle I(hkl) \rangle| / \sum_k \sum_l I(hkl)$   
 $R_{\text{work}} = \sum |F_{\text{obs}}| - |F_{\text{calc}}| / \sum |F_{\text{obs}}|$   
 $R_{\text{free}} =$  as for  $R_{\text{work}}$ , but calculated for 5.0% of the total reflections that were chosen at random and omitted from refinement

**TABLE 1:** Statistics of X-ray diffraction data collection and structure refinement. Key: values in parentheses are for the highest resolution shell (1.9–1.8Å).

FhuD2<sub>27-302</sub> mainly presents 35.7% of alpha helix, 7.9% of G-helix and 19.9% of  $\beta$ -strands (Fig 7 and Fig 8).

In particular, the topology of secondary structure shows three  $\beta$ -sheets elements, formed by thirteen  $\beta$ -strands. Sheet A contains two strands antiparallel of five residues each; Sheet B presents five strands parallel, two elements composed of three amino acids, two elements composed of five amino acids and one composed of four amino acids. Sheet C contains six strands mixed of 8-5-2-3-4-3 residues, respectively, (Fig 7 and Fig 8). FhuD2 presents 17 helices that are composed of six

G- type helix and eleven H-type helix, eight of them are positioned into the N-lobe, eight into the C-lobe and one connecting the two main globular domains (Glu149-Ile174).

```
MKAETKSYKMDDGKTVDIPKDPKRIAVVAPTYAGGLKKLGANIVAVNQVVDQSKVLKDKFKGVTKIGDGDVEKVAKEKPD  
LIIVYSTDKDIKKYQKVAPTVVVDYNNKHKYLEQQEMLGKIVGKEDKVKAWKKDWEETTAKDGEIKKAIGQDATVSLFDEF  
DKKLYTYGDNWGRGGEVLYQAFGLKMQPEQQKLTAKAGWAEVKQEEIEKYAGDYIVSTSEGKPTPGYESTNMWKNLKA  
TKEGHIVKVDAGTYWYNDPPTLDFMRKDLKEKLIKAAK
```

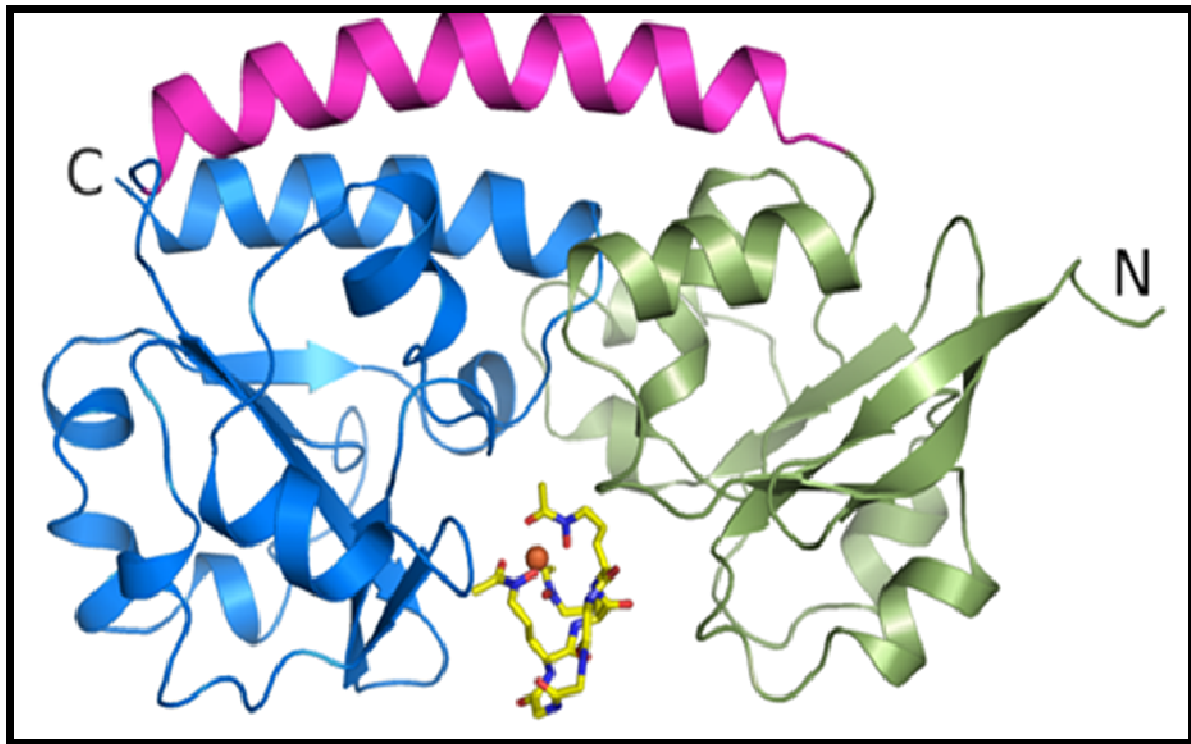


**FIG 6:** A ribbon representation revealing iron (III) ferrichrome (shown as sticks; yellow: carbon, blue: nitrogen, red: oxygen) bound between the N-terminal lobe (green) and C-terminal lobe (blue) of FhuD<sub>27-302</sub>. The two lobes are connected by a long  $\alpha$ -helix (magenta). The single Fe<sup>3+</sup> ion (red sphere) is caged within the ferrichrome.



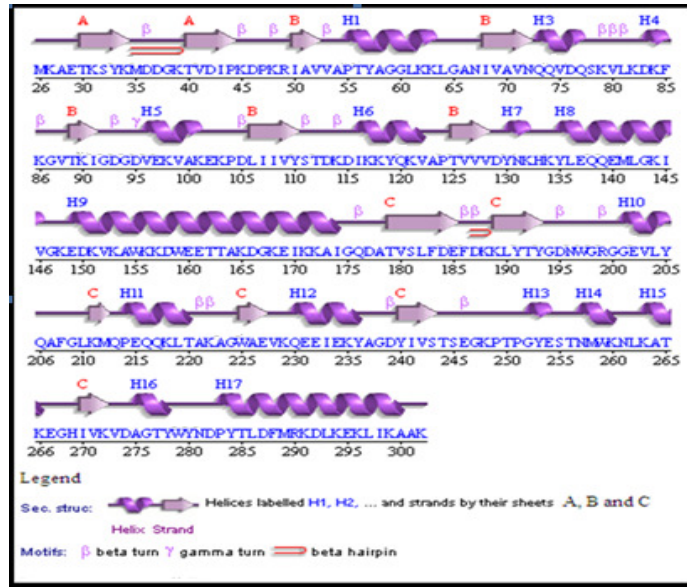


FIG 7: schematic representation of secondary structure

There are also four beta-alpha-beta units, which consist of two parallel hydrogen bonded beta strands connected by a loop containing at least one alpha helix, between residues Ile50-Asn72, Leu106-Val128, Lys211-Glu227 and Tyr240-Lys272. In addition we can observe also the presence of two beta hairpin elements, which are motives consisting of two strands that are adjacent in primary structure and oriented in an antiparallel arrangement linked by a short loop (Fig. 7); beta hairpins belong to class 3:5 (Thr30-Pro44) and 2:2 (Thr179-Tyr193).

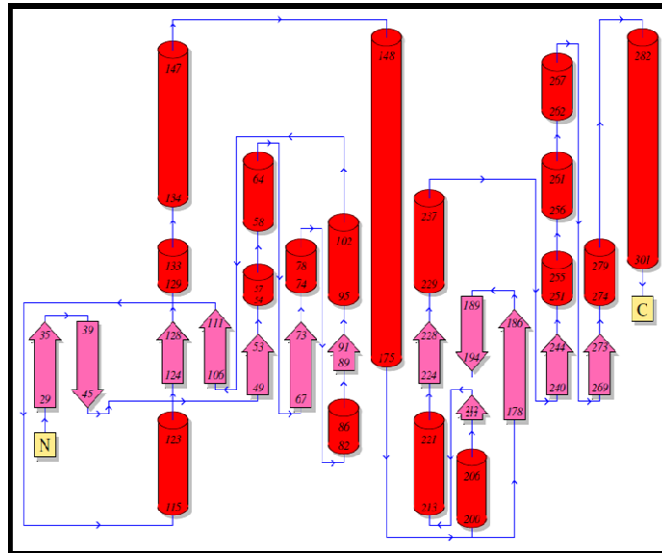
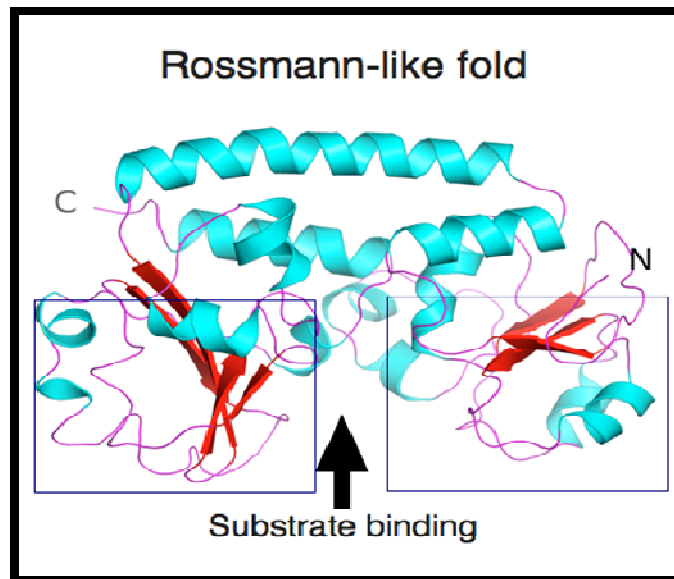


FIG 8: Secondary structure topology diagram for FhuD<sub>27-302</sub>

In the secondary structure are present two  $\beta$ -bulges, region of irregularity in a  $\beta$ -sheet involving two  $\beta$ -strands, which are comprised of two or more residues in the bulged strand opposite to a single residue on the adjacent strand [87]. Residues involved in the two  $\beta$ -bulges of FhuD2 are Met35, Gly38 and Lys39 (antiparallel G1 type) for the first and Ile50, Ile68 and Val69 (Parallel classic type), for the second. An overall view of the secondary structure reveals also the presence of 21  $\beta$ -turns, regions of the protein involving four consecutive residues where the polypeptide chain folds back on itself by nearly 180 degrees, [88, 89] [90] [91] [92]; and of a  $\gamma$ -turn, a type of non regular secondary structure that causes a change in direction of the polypeptide chain, (Fig 7). The polypeptide chain links the N-Terminal and C-Terminal domains, connecting them via a unique 25-residue  $\alpha$ -helix that runs the entire length of the protein. It is also possible to note that the  $\alpha/\beta$  structural units on C and N-lobe of the protein form two distinct tertiary structures and the architectures of these domains can be placed in the family of Rosmann-like folds , one for each lobe [93] (Fig 9).



**FIG 9:** Schematic representation of the two Rosmann-like folds

Atomic displacement parameter in protein crystal structures reflects their flexibility and dynamics, based on the fluctuation of atoms about their average position [94]. A large B-factor is typical signal of high mobility of individual atoms and side chains, whereby FhuD<sub>27-302</sub> structure presents a restricted and well defined region corresponding to the active site where B-factor is low. This shows the active site in the interface of N- and C-domains as a very well ordered region of the protein, in comparison to the two lateral lobes (Fig 10).

Different parts of the same molecule may exhibit different degrees of polarity according to their structure and amino acid composition, from highly hydrophilic to totally hydrophobic. Projection of these differences onto the molecular surface gives rise to a hydrophobicity map. Hydrophobicity maps show the tendency of

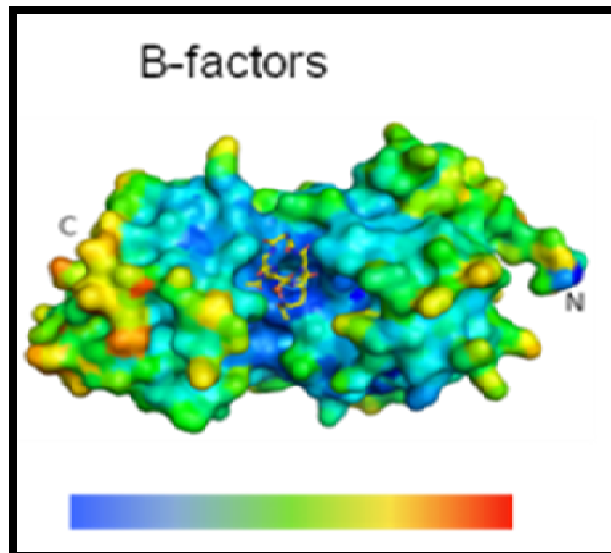


**FIG 10:** B factors distribution from low (blue) to high (red)

atoms or groups of atoms to interact with water according to their chemical nature, their placement inside the molecule and the functional groups to which they belong (<http://www.arpe.snv.jussieu.fr/>). These models allow the prediction of the behavior of a molecule when solved in water or in an organic solvent. Observing the FhuD2 hydrophobicity map, it is possible to appreciate that the density of hydrophobic residues remains consistently low, but increases significantly into the region encompassing the ligand binding site (Fig 11). In addition, the electrostatic potential map of the surface of the FhuD2 reveals that the protein presents superficial areas with an high level of electrostatic charge, mostly represented in blue (positive) in the Fig 12. It is still interesting that FhuD2<sub>27-302</sub> hides an internal electrostatic interface between N- and C-domains, where N-lobe has an high level of positive charge, while the C-lobe shows an high level of negative charge. This internal electrostatic surface at the domain interface is possibly responsible for lobes interaction (Fig 12).

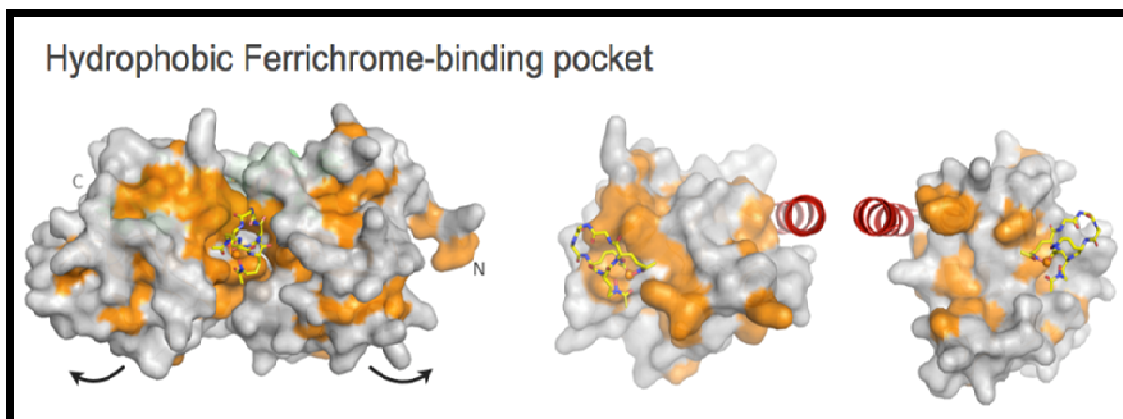


**FIG 11:** A surface plot of FhuD2 with hydrophobic regions colored orange

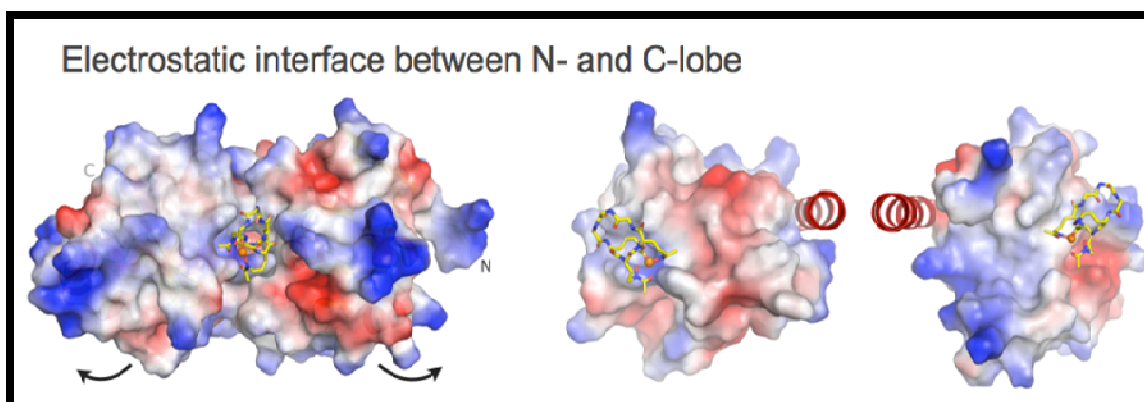


**FIG 12:** Electrostatic surface plots of the highly-charged interface between the N- and C-terminal lobes of FhuD2<sub>27-302</sub>. Positively-charged (blue) residues on the N-terminal lobe (right) interact with negatively-charged (red) residues on the C-terminal lobe (left)

Structural comparisons between FhuD2<sub>27-302</sub> and its structural homologs, both in the apo and holo forms, are shown in Table 2. As shown in Fig. 13, the superposition performed by SSM (Secondary Structure Matching) shows a conserved overall architecture.

Accordingly, the FhuD2 fold can be closely superimposed with the structures of several previously determined homologues of the Class III Binding Protein family [50, 61], with overall root mean square deviation (rmsd) scores for ~260 aligned C $\alpha$  atoms ranging from 2.2-2.8Å for *S. aureus* SirA [95], *B. subtilis* BSU3320, *S. aureus* HtsA [35], *E.coli* FitE [96], *E. coli* FhuD [58] and *B. subtilis* FeuA [97]. Moreover, if the N- and C-terminal lobes are treated separately, rmsd scores as low as 1.3Å can be obtained, e.g. by independently superposing the two lobes of FhuD2 onto BSU3320. Nonetheless, the FhuD2 structure is only the second Binding Protein structure determined in the presence of the naturally-occurring Fe<sup>3+</sup>-chelator ferrichrome, and is the first example of a hydroxamate siderophore Binding Protein from *S. aureus*.

<b>Sequences producing significant alignments</b>	<b>Organism</b>	<b>Max % Identity</b>
3HXP Iron(3+)-hydroxamate-binding protein fhuD	<i>B. Subtilis</i>	38.5
3G9Q Ferrichrome-binding protein	<i>B. Subtilis</i>	38.1
3GFV Uncharacterized ABC transporter solute-binding protein yclQ	<i>B. Subtilis</i>	29.9
3MWG Iron-regulated ABC transporter siderophore-binding protein SirA	<i>S. Aureus</i>	27.6
3MWF Iron-regulated ABC transporter siderophore-binding protein SirA w/ staphyloferrin	<i>S. Aureus</i>	27.6
2PHZ Iron-uptake system-binding protein	<i>B. Subtilis</i>	27.6
2XV1 IRON-UPTAKE SYSTEM-BINDING PROTEIN WITH FERRIC MECAM	<i>B. Subtilis</i>	26.9
2WHY IRON-UPTAKE SYSTEM-BINDING PROTEIN WITH FERRI-BACILLIBACTIN	<i>B. Subtilis</i>	26.9
2XUZ IRON-UPTAKE SYSTEM-BINDING PROTEIN WITH FERRI-ENTEROBACTIN	<i>B. Subtilis</i>	26.9
2WI8 IRON-UPTAKE SYSTEM-BINDING PROTEIN	<i>B. Subtilis</i>	26.9
3LHS Ferrichrome ABC transporter lipoprotein complexed with Staphyloferrin A	<i>S. Aureus</i>	25.4
3LI2 Ferrichrome ABC transporter lipoprotein Complexed with Staphyloferrin A	<i>S. Aureus</i>	25.4
3E1W HtsA protein	<i>S. Aureus</i>	25.4
3E1X HtsA protein/selenomethionine labelled	<i>S. Aureus</i>	25.4
2X4L FERRIC-SIDEROPHORE RECEPTOR PROTEIN	<i>S. coelicor</i>	24.6
3BE5 Putative iron compound-binding protein of ABC transporter family	<i>E.coli</i>	24
3BE6 Putative iron compound-binding protein of ABC transporter family	<i>E.coli</i>	24

**TABLE 2:** Comparative analysis of the structures deposited in the PDB that have a higher than 24% identity with *S. aureus* FhuD2

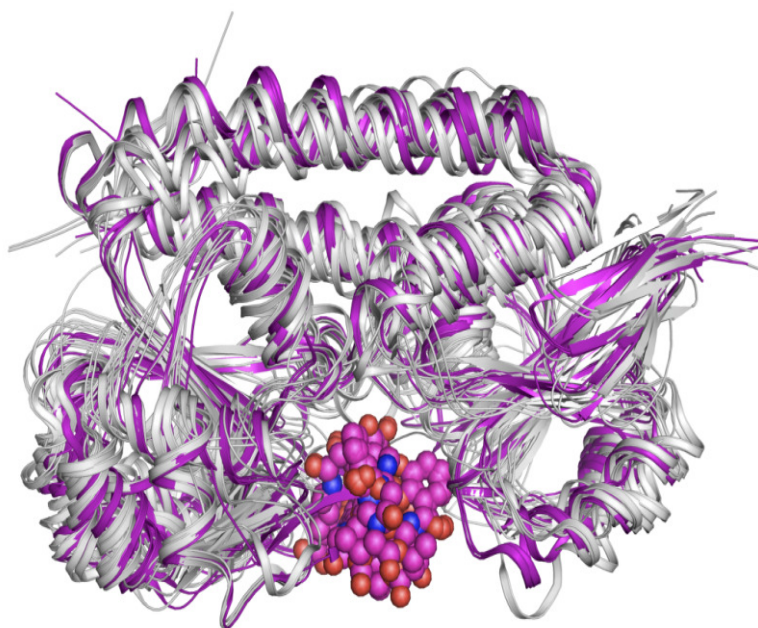


**FIG. 13:** Protein structure comparison on secondary structure matching (SSM) of FhuD2 homologs showed in tab1. Color scheme: protein homologs in holo-form (violet), protein homologs in apo-form (gray)

## *A network of polar and hydrophobic interactions form the groove*

*where FhuD2<sub>27-302</sub> captures ferrichrome*

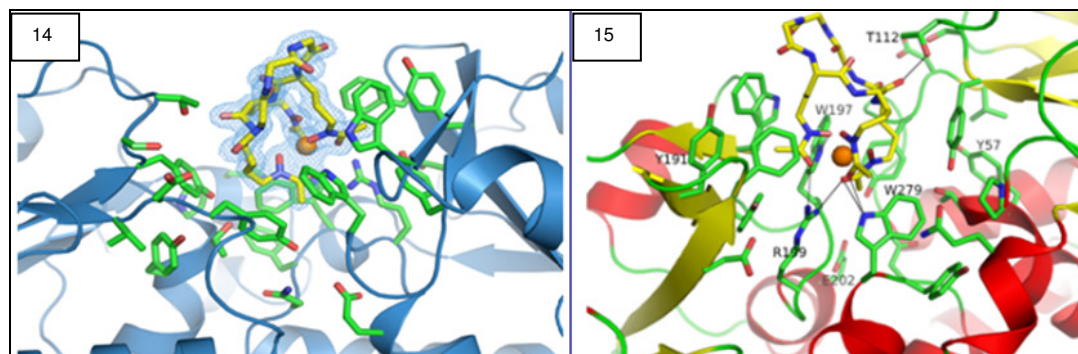


**FIG 14:** Ferrichrome density map and side chains of residues lining the cavity where ferrichrome is bound. The conformation of the iron-loaded ferrichrome is clearly visible in the sigma weighted 2IFol-IFcl electron density map, here contoured at 1.3  $\sigma$ .

**FIG 15:** Polar and hydrophobic interactions forms the groove where FhuD2<sub>27-302</sub> captures ferrichrome. Residues involved in polar interactions (dashed lines) between the protein and ferrichrome are labeled (T112, W197, W279, R199), as well as residues known from literature to be important for siderophore binding (Y191, W202, Y57, W197). Ferrichrome binding site is depicted as cartoon, colored according to its secondary structure elements (helices in red, sheets in yellow, and loops in green)

Side chains of hydrophobic residues line the inner walls of the cavity of ferrichrome binding site, as is clearly illustrates in Fig 14. The binding site is composed mostly of hydrophobic residues (Fig 11, 14 and 15). At the base of the binding pocket, where ferrichrome is located, it is possible observe the presence of three FhuD2 residues, all positioned on the C-terminal lobe, that interact directly with ferrichrome using hydrogen bond, Trp197, Arg199 and Trp279 respectively; all are contributed by the C-terminal lobe. One of these, Arg 199, with its side chain  $-NH_2$  groups, seems to be positioned into the architecture of the active site, with distances such as to permit multiple hydrogen bonds, precisely with all three hydroxamate carbonyl groups of ferrichrome, by placing as central component of ligand binding.



However also the side chain – NεH groups of Trp197 and Trp279 are able to form H-bonds with the same carbonyl oxygens used by Arg 199, indicating how a web of polar bonds is the basis of the link with the siderophore.

Observing the iron atom, directly bound and stabilized with the common octahedral coordination, in this case using three bidentate hydroxamate groups of ferrichrome, it is immediately clear how the protein does not form any kind of direct interaction with the Fe<sup>3+</sup> ion.

Moving the focus in the upper edge of the cavity, it can be noted as a fourth residues (Thr 122) belonging at N-terminal lobe, but with a more peripheral position than the other two, using its side chain hydroxyl group to form an H-bond by engaging a carbonyl group of one of the six peptide moieties of ferrichrome.

In addition to these residue-specific H-bonds, the binding of ferrichrome is also stabilized by a number of van der Waals' packing interactions, involving hydrophobic moieties of Tyr110, Tyr130, Phe186, Tyr191, Trp197, and Trp225. Collectively, this network of interactions appears to endow FhuD2 with a strong and specific recognition pattern for ferrichrome.

The residues involved in polar interactions (T112, W197, W279, R199) shown in Fig 15 have been aligned to determine if they are conserved in the homologous (tab 3) and the most significant have been structural represented in the figure 16.

```

fhuD2/26-302 26 MK-----AETKSYKMDDGKTVDIPKDPKRIVAVVAP 55
fhuD1/1-303 1 MKRLIGILLCNLFI L T ACSASVDKTSNSTKT TDYK I ENGETLKVPEKPKRVAVLTG 56
3HXP/24-316 24 MGN-----NSESKGSASDSKGAETFTYKAENG-NVKIPKHPKRVVVMAD 66
3MWG/52-329 52-----GSKRVVTLTYQ 61
3LHS/32-331 32-----GSHMASTISVKDENG-TVKVPKDAKRIVVLEY 62

fhuD2/26-302 56 TYAGGLKKLGANIVAVNQVQDQSKVLK---DKFKGVTKIGDGD---VEKVAKKPD 105
fhuD1/1-303 57 FYVGFDFIKLGIKPIAVSDITKDSSILK---PYLKGVDYIGEND---VERVAKAKPD 106
3HXP/24-316 67 GYYGYFKTLGINVVGAPENVFKNPYYK---GKTNGVENIGDGT---VEKVIDLNP 117
3MWG/52-329 62 GATDVAVSLGVKPVGAVESWTQKPKFEYIKNDLKDITKIVGQEPAPNLEEISKLKPD 117
3LHS/32-331 63 SFADALAAIDVKPVGIAADDGKKRIIKPVREKIGDYTSVQTRKQPNLEEISKLKPD 118

fhuD2/26-302 106 LIIVYSID-KDIKK-YQKVAPT VVVDY NKHKYLEQQ---EMLGKIVGKEDKVKAWK 156
fhuD1/1-303 107 LIVVDAD-KNKK-YQKIAPTIPYTYNKYNHKEIL---KEIGKLTNNEDKAKKWI 157
3HXP/24-316 118 LIIVWTIQGADIKK-LEKIAPTVAVKYDKLDNIEQL---KEFAKMTGTEDKAEKWL 169
3MWG/52-329 118 LIVASKVREKYYDQLSKIAPTVSTDT-VFKFKDIT---KLMGKALGKEAEEDLL 169
3LHS/32-331 119 LIIDSSRHGKINKELNKIAPTL S LK SFDGDYKQIN S F K T I A K A L N K E K E G E K R L 174

fhuD2/26-302 157 KDWEETTAKDGKEIKKAI GQDATVSLFDEFDKKLYTYGDNWFRGGEVLYQAFGLKM 212
fhuD1/1-303 158 EEWDDKTRKDKKEIQSKIGQ-ATASVFEPDEKQIYIYNSTWFRGLDVHDAFGMPM 212
3HXP/24-316 170 AKWDDKVA AAKTKIKKAVGD-KTISIMQTNGKDIYVFGKDFRGGSIYKDLGLQA 224
3MWG/52-329 170 KKYDDKVA AAFQKDAKAKYKDAWPLKASVVNFRADHTRIYAGGVAGEILN-DLQFKR 224
3LHS/32-331 175 AEHDKLINKYKDEIKFDRNQKVLPAVVAKAG--LLAHPNYSYVQFLNELGFKNAL 228

fhuD2/26-302 213 QPE-QQKLT-AKAG-WAEVQEEIEKYAGDYIVST--SEGKPTPGY-----ES 255
fhuD1/1-303 213 TKQYKDKLQEDKKG-YASISKENISKYAGDYIFLS--KPSYGKDFD-----EK 257
3HXP/24-316 225 T K L T K E K A I D Q G P G - Y T S I S L E K L P D F A G D Y I F A G P W Q S G G D D G G V - - - - - F E 271
3MWG/52-329 225 NKDLQKQVD-NGKDIQLTSKESIPLMNADHIFVVKSDPNAKDAALVKKTESEWTS 279
3LHS/32-331 229 SDDVTKGLSKYLKGPYLQLDTEHLADLNPERMIIMTDHAKKDSAEFKKL----QE 279

fhuD2/26-302 256 TNMWKNL KATKEGHI-VKVDAGTYWYNDPYTLDFMRKDLKEKLIKAAK----- 302
fhuD1/1-303 258 THYWNIEAVKKGHV-ISYKAEDYFTDPIITLEHLRSKLKKEILNKK----- 303
3HXP/24-316 272 SSWKNLNAVKNQGHV-YKMDPIGFYFTDPI SLEGLEFITESLTKLEHHHHHH 323
3MWG/52-329 280 SKEWKNLDAVKNNQVSDLDL E I T W N L A G G Y K S S L K L I D D L Y E K L N I E K Q S K - - 330
3LHS/32-331 280 DATWKKLNAVKNRNV-DIVDRDVAARSRLISSEEMAKELVELSKKEQK---- 327

```

TAB 3: Alignment of the amino acid sequence of FhuD<sub>27-302</sub> with *S. aureus* FhuD1 and most relevant homologs selected for the superimposition analysis: FhuD fold-family BSU3320 from *B. subtilis* (PDB code 3HXP), SirA from *S. aureus* (PDB code 3MWG) and HtsA from *S. aureus* (PDB code: 3LHS)

The comparison shows a high level of difference in all four residues involved in binding. In detail, FhuD1 shows a sequence identity in W197, W279 and R199, but only BSU3320 from *B. subtilis* (PDB code 3HXP) shows a slightly structural identity on the residues involved in ligand binding: T112 and R199.

Another important element that emerges from the structure is where are the real position of the amino acids (E97 and E231) involved in interaction with ABC transporter. As it was hypothesized by Sebulsky the two glutamic acids should be particularly exposed, on the N- and C- lobes respectively, in order to permit an easy interaction with the ATPase [65, 71]. In fact, as shown in Fig 17 the two glutamic acids are positioned at the summit of the two globular domains.

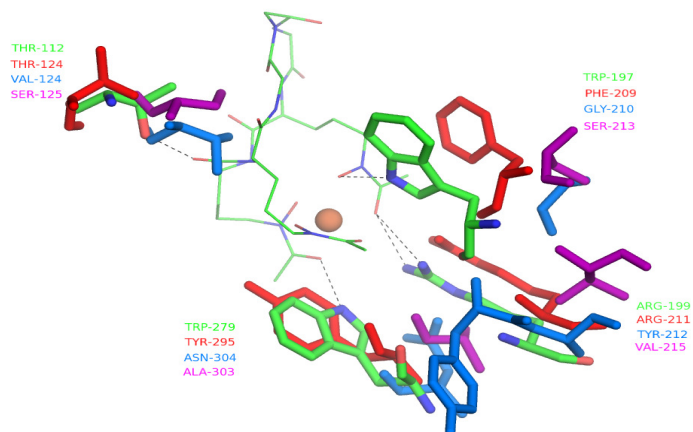


**FIG 16:** structural comparison of amino acids involved in FhuD2<sub>27-302</sub> siderophore binding with residues known in literature as responsible of substrate interaction. FhuD2 colored in green, 3HXP in red, 3MWG in blue and 3LHS in violet.

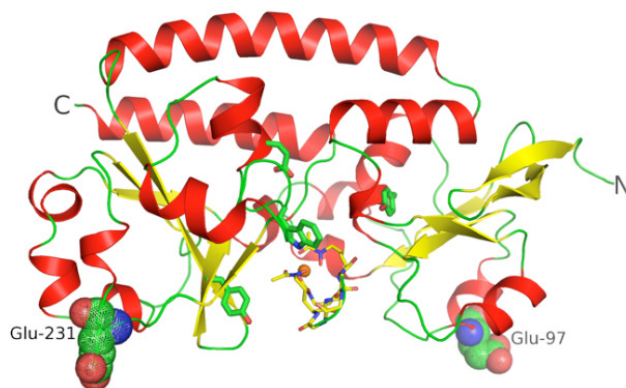


**Fig 17:** Stereo view of amino acids known from the literature to be necessary for the interaction with the ABC transporter

***High-affinity, iron-dependent binding of ferrichrome to FhuD2 in SPR assays***

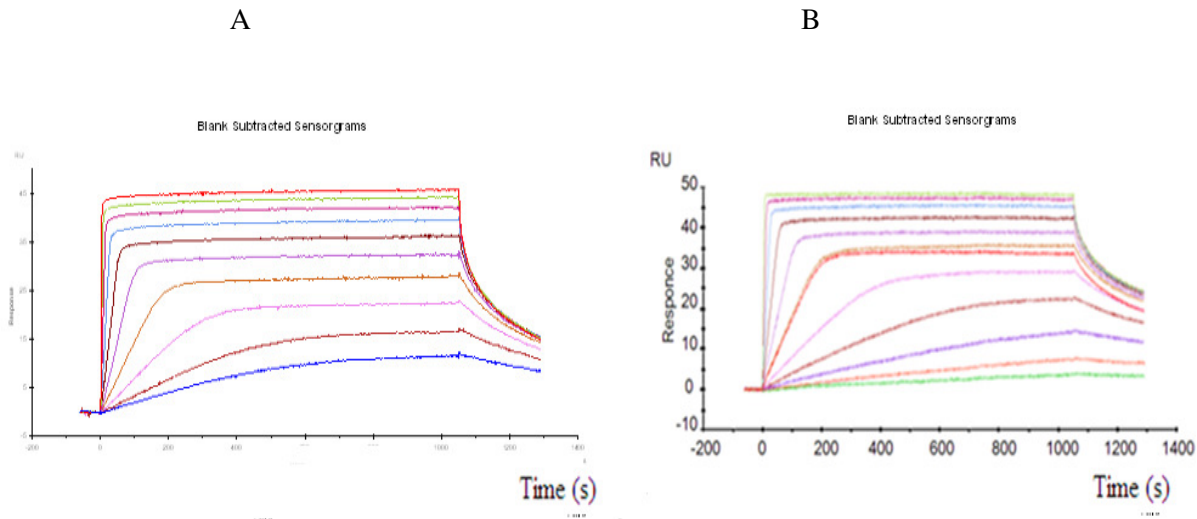


**FIG 18:** Affinity of FhuD2<sub>18-302</sub> and FhuD2<sub>27-302</sub> for Ferrichrome.

SPR measurements of the kinetics ( $k_{on}$ ,  $k_{off}$ ) and equilibrium dissociation constant ( $K_D$ ) of the FhuD2-ferrichrome interaction, calculated from steady-state analysis using as parameter the binding between CM5 chip immobilized recombinant FhuD2<sub>18-302</sub> and FhuD2<sub>27-302</sub> with ferrichrome (injected at increasing concentrations, from 1nM to 1mM) have shown very fast association and dissociation rates falling in a low nanomolar affinity range for both proteins ( $K_d = 9$  nM), not dissimilar from the value previously obtained from intrinsic fluorescence quenching analyses (20nM) [71].

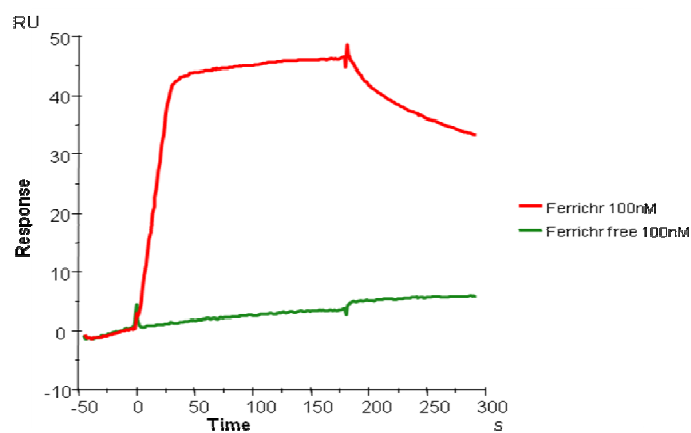


**FIG 19:** FhuD2<sub>18-302</sub> did not present the same range of affinity with Ferrichrome-iron free

Collectively these data, show that the two proteins may be considered identical in terms of specific binding activity. Therefore, the 12 AA N-terminal fragment is not involved in any receptor-siderophore binding activity.

SPR of the interaction between the recombinant receptor FhuD2<sub>18-302</sub> with iron-free ferrichrome (injected at the same conditions) did not show any interaction, indicating the strict dependence on the presence of the metal for the protein binding.

## *Interaction between transferrin and iron-free ferrichrome*

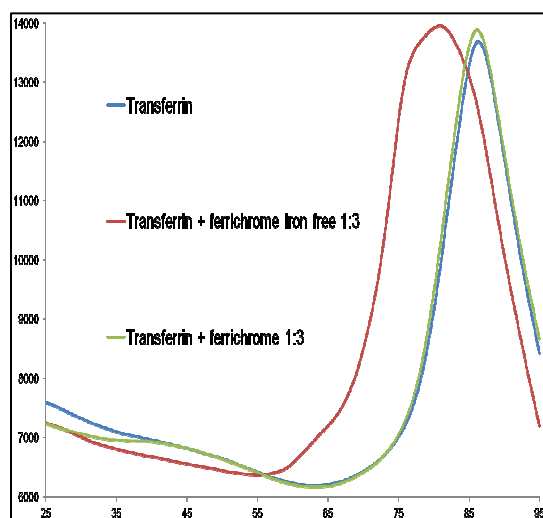


**FIG 20:** Thermal stability decrease of transferrin caused by addition of iron-free ferrichrome

Of the approximate 3 grams of body iron in the adult male, approximately 3 mg or 0.1% circulates in the plasma. Essentially all circulating plasma iron normally is bound to transferrin. This chelation serves three purposes: it renders iron soluble under physiologic conditions, it prevents iron-mediated free radical toxicity, and it facilitates iron transport into cells. Transferrin is an 80 kDa glycoprotein with homologous N-terminal and C-terminal iron-binding domains [98] and is considered the most important physiological source of iron for red cells [99, 100]. The liver synthesizes transferrin and secretes it into the plasma. Transferrins are produced locally in the testes and CNS [101]. To test the possibility that siderophore used by FhuD2 are able to strip iron from transferrin for a possible bacterial usage, we performed a Differential Scanning Fluorimetry (DSF) with

human transferrin and various siderophores with and without iron. The presence of iron free ferrichrome significantly changes thermal stability of transferrins as measured by DSF ( $\Delta T_m \sim 8$  °C) (Fig. 20). Transferrin, [102], in our experiments has displayed a high melting temperature ( $\sim 82$ °C), which has been sensibly reduced by increasing amounts of iron-free ferrichrome. This destabilizing effect is likely generated by Fe(III)-uptake by ferrichrome directly from transferrin, confirming its major affinity for Fe(III) compared with transferrin. In contrast, ferrichrome (iron-loaded) had no effect on the  $T_m$  of transferrin.

# DISCUSSION

Iron is an important micronutrient for virtually all living organisms, only lactic acid bacteria use manganese and cobalt in place of iron. Iron can be incorporated into specific proteins and therefore is involved in many biological processes such as photosynthesis, respiration, the tricarboxylic acid cycle, oxygen transport, gene regulation, DNA biosynthesis, etc. [61].

The reaction of Fenton, which involves the powerful oxidant formed from ferrous salts plus  $H_2O_2$  in acidic aqueous solution, first described a century ago (Fenton, H. J. H. 1894, J. Chem. Soc. 65, 899-910.), produces the hydroxyl radical ( $\cdot OH$ ), which is generally associated as the primary intermediate of such aqueous oxidations and the main cause of oxidative cell damage [103],[104]. In fact the formation of the highly reactive and hence cytotoxic, free hydroxyl radical has a critical impact to living organisms [105]. It can lead to formation of highly toxic species of oxygen that can be very harmful for the organism, thus a mechanism of “iron-control” is necessary. This mechanism decreases the cellular concentration of the ferric ion to a value insufficient for microbial survival. To overcome this nutritional limitation, microorganisms are able to use extracellular forms of transferrin and lactoferrin or precipitated ferric hydroxides [61].

Intracellular bacteria typically use siderophores to obtain iron from hemoglobin [106]. Evolution has led to the formation of two main methods of acquisition of iron, schematically represented as: (i) iron acquisition by cognate receptors using low molecular weight iron chelators termed siderophores or (ii) receptor-mediated



iron acquisition from host proteins. These two mechanisms are necessary because the most common channels for solute acquisition are the trimeric  $\beta$ -barrel proteins, termed porins, immersed into the outer membrane and these work only with solutes of up to 600 Da. Therefore transferrin or lactoferrin cannot utilize this transmembrane channel and other mechanisms are necessary.

Bacteria normally use specific binding proteins that act as siderophore receptors, which are commonly termed PBP super-family proteins (Periplasmic Binding Proteins), due to their initial identification in the periplasm of Gram-negative bacteria. In Gram-positive bacteria, PBPs are membrane-anchored and exposed to the extracellular milieu. In each case PBPs work with specific ABC transporters to mediate active transport (internalization) of their ligands.

Historically the classification of PBPs has been object to many changes. It was proposed that the individual domains of PBPs could have arisen by the mixed  $\alpha/\beta$  ancestor protein CheY, and the two-domain architecture is due to a domain dislocation event rather than domain swapping [107]. Starting from Tam and Saier [108], through Quioco [51] and Claverys [109] until arriving to Chu and Vogel[50], there have been many revisions about how to classify this protein super family. Many classification criteria have been used, such as sequence similarity or molecular weight but all methods showed large variability: 20–75 kDa and 20%, respectively. Finally, the Binding Proteins have been divided into three classes and although they exhibit varying sizes they share a similar tertiary structure organization composed of two distinct globular domains separated by a central groove, thus creating a bilobate structure tailored for ligand binding. Class I and II share three major common structural features: (1) they consist of two distinct globular domains of mixed  $\alpha/\beta$  structure separated by a shallow or deep binding

cleft; (2) the substrate is bound in the cleft with either a shallow or deep binding mode; (3) the hinge-bending motions between the two domains provide the substrate with access to the binding pocket [51]. About ten years ago, the first structural studies reporting a new class of PBP emerged, featuring *E. coli* FhuD [58] and *T. pallidum* TroA [110], [111]. This last group of fold has been described having domains consisting of a central  $\beta$ -sheet flanked by  $\alpha$ -helices and a long  $\alpha$ -helical linker that connects the two domains [50]. Unlike the Class I and II Binding Proteins that feature a central hinge region, the Class III proteins are folded such that the two lobes meet in a relatively large complementary interface that seems to confer more rigidity to the protein causing the lacking of a large structural change when the protein is bound to ligand. The large conformational rearrangement of Class I and II PBPs is commonly named Venus fly trap mechanism.

Vogel in a closer examination of class III PBPs, denoted structural differences into this group and subdivided the class III into two subclasses that have as “prototypes” *E. coli* FhuD or *T. pallidum* TroA. In the case of FhuD-like proteins, each domain has a central mixed or parallel orientation  $\beta$ -sheet consisting of three to nine  $\beta$  strands with the C-terminal domain  $\beta$ -sheet adopting a twisted conformation [50]. In comparison, TroA-like PBPs that bind zinc or manganese all have twisted four-stranded  $\beta$ -sheets in both domains. Another noticeable difference between these type III subtypes is that the domain-spanning  $\alpha$ -helix linker averages 25 residues in TroA-like folds and 20 residues in FhuD-like PBPs. In addition, a two to three residue  $3_{10}$ -helix is consistently found leading into the interdomain linker of the TroA-type PBPs [50]. We performed a detailed study of the class III Binding Protein FhuD2 from *S. aureus*, which we recently described as a potential vaccine antigen (R. Mishra et al 2012).

*S. aureus* FhuD2 is linked to the membrane by a lipid anchor covalently bonded to a crucial Cys residue located in the conserved 'lipobox' of its signal peptide, Cys 18. The N-terminal segment also acts as a flexible spacer that renders FhuD2 accessibly exposed on the outer bacterial surface. Biochemical and structural studies were principally based on two clones: FhuD2<sub>18-302</sub> and FhuD2<sub>27-302</sub>, both of which lack the putative N-terminal signal peptide predicted to contain a high level of disorder and flexibility (Fig 2). The FhuD2 proteins from NCTC8325 *S. aureus* strain were expressed cytoplasmically in *E. coli*, purified to homogeneity and purity was tested by Reverse-Phase chromatography, showing a value of 98% for each protein.

Circular dichroism spectroscopy of FhuD2<sub>18-302</sub> and FhuD2<sub>27-302</sub> revealed the same predominantly  $\alpha$ -helical secondary structures, demonstrating the structural similarity of the two constructs and that the deletion of the 26 N-terminal residues, predicted to be disordered, does not prevent the correct folding (Fig 3 and 4A). Since N-terminally-truncated has been used, well-folded recombinant proteins was a crucial parameter in the rational design of the project.

The overall thermal stability and functional integrity of FhuD2 were examined using differential scanning fluorimetry (Fig 4). DSF experiments, revealing the mid-point of a protein melting transition ( $T_m$ ) via a chemical probe, have shown that both FhuD2 constructs have the same thermostability range ( $T_m$   $51.6 \pm 0.1$  °C). For both constructs, the stability was dramatically enhanced to a  $T_m$  of  $66.1 \pm 0.4$  °C by addition of iron(III)- hydroxamate siderophores (ferrichrome), know in literature have a high affinity for *S. aureus* FhuD2 [47, 65, 71], but not for catecholate siderophores or hemin.

Ferrichrome makes several hydrophobic contacts with FhuD2 and multiple H-bonds from the hydroxamate groups to key residues (described below) derived from both

the N- and C-terminal lobes(Fig 11,14 and15); this domain-bridging effect is likely to underlie the enhanced thermostability observed in the presence of ferrichrome (Fig 4).

In order to obtain high resolution information of FhuD2 we used the highly purified apo-FhuD2, but unsuccessfully. Therefore, we performed co-crystallization in the presence of a few siderophores: coprogen, aerobactin and ferrichrome, respectively. Using this rational design of the crystallization experiments we rapidly obtained strongly diffracting crystals of FhuD2<sub>27-302</sub> bound to ferrichrome (Fig 5) [50], [61].

The structure was determined by molecular replacement, using as a search model the atomic coordinates of the FhuD2 structural homologue from *B. subtilis* (PDB code: 3G9Q), with which FhuD2 shares 38% overall sequence identity. The structure was refined against 1.8Å resolution data with final values of  $R_{\text{work}}$  and  $R_{\text{free}}$  factors of 19% and 23.2%, respectively (Tab 1). The overall structure of *S. aureus* FhuD2<sub>27-302</sub> revealed all the hallmarks of a Class III family Binding Protein: two lobes positioned at the N- and C-termini, respectively, and linked by a helix (E149-A173) which connects the two protein regions with ferrichrome harbored in the central cavity (Fig 6).

Each globular domains, present a Rossmann-like fold and specifically the N-terminal lobe exhibits a central six-stranded  $\beta$ -sheet surrounded by six short  $\alpha$ -helices and the C-terminal lobe has a five stranded  $\beta$ -sheet surrounded by seven short  $\alpha$ -helices (Fig 9). The bilobate bean-like structure binds the ligand, iron (III) ferrichrome, in a cleft approximately 17 Å deep, located between the N- and C-terminal lobes (Fig 6 and 14).

The overall fold is shared by homologues of FhuD2 for which the structures are known, including: BSU3320 from *B. subtilis* (PDB code 3HXP), SirA from *S.*

*aureus* (PDB code 3MWG), Dese from *S. coelicor* (PDB code 2X4L) [112], and FitE from *E. coli* (PDB code 3BE5) [96]. Collectively, these structures are typical of the class III PBPs (Fig 13), underlining other aspects of *S. aureus* FhuD2 structure, such as the extensive, buried interface, (Fig 12), dominated by polar and electrostatic inter-domain interactions or the characteristic long  $\alpha$ -helix, here formed by 25 residues which together, would seem to render the overall protein somewhat rigid (Fig 6).

Despite low pairwise sequence identities (15-35%), the FhuD2 structure can be readily superposed onto apo- and ligand-bound forms of numerous homologous protein from various species, with rmsd scores of 2.2-2.8Å, generated by SSM. These structural similarities, together with CD spectroscopy and SAXS data reported previously for FhuD2 [71], suggest that FhuD2 is unlikely to undergo significant local or global conformational changes upon ligand binding, in keeping with the current model for most class III Binding Proteins. However, in the absence of the ligand-free structure of FhuD2, some doubt remains over the potential for a siderophore to trigger a minor open-to-closed rearrangement.

The structure of FhuD2<sub>27-302</sub> bound to iron (III) ferrichrome reveals a network of polar and hydrophobic residues, which form the binding pocket responsible of the specific protein-siderophore interaction. In more detail, Ferrichrome binds FhuD2 in a relatively hydrophobic cavity located between the two lobes and is only partially buried, in this shallow binding pocket. By remaining partially solvent-exposed, ferrichrome may subsequently participate directly in the interaction between FhuD2 and its membrane-bound receptor, in contrast with those ligands that are fully engulfed by their Class I or II Binding Proteins.

While the ferrichrome is directly bound to the iron atom via octahedral coordination, by the six oxygens of the three ferrichrome hydroxamate moieties, FhuD2 forms contacts only with the siderophore and does not chelate  $\text{Fe}^{3+}$  directly. The high-affinity FhuD2-ferrichrome interaction is iron-dependent, as shown by surface plasmon resonance (SPR) experiments performed in an attempt to investigate the kinetics ( $k_{on}$ ,  $k_{off}$ ) and equilibrium dissociation constant ( $K_D$ ) of the FhuD2-ferrichrome interaction. The results revealed very fast association and dissociation rates that prevented reliable fitting of the sensorgrams with any of the standard kinetic models of Langmuir interactions. Therefore a steady-state analysis was used to obtain  $K_D$  values from a plot of the equilibrium binding response ( $\text{Req}$ ) against ferrichrome concentration. For iron (III) ferrichrome, the interaction with FhuD2 revealed a  $K_D = 9\text{nM} \pm 0.5\text{nM}$ . Despite the lack of direct interactions between the  $\text{Fe}^{3+}$  ion and the protein, the binding of ferrichrome was shown to be strictly dependent on the presence of the metal, since deferrichrome (ferrichrome lacking iron) did not interact significantly with FhuD2.

Analyzing the interaction between FhuD2 and its ligand it is possible to distinguish a trio of FhuD2 residues (Trp197, Arg199, Trp279) at the base of the binding pocket and one more peripheral, (Thr112), positioned at the top of the cleft, which all make multiple H-bonds to the ferrichrome hydroxamate groups, that collectively assume key roles in ligand binding (Fig 15). Also Van der Waals interactions of these and other hydrophobic residues contribute to affinity by interacting with the methylene groups of the ornithine moieties, but only the H-bonds present a central role in conferring ligand specificity. This observation is supported also by data from literature, [71], where FhuD2 W197A mutant loses ability to bind ferrichrome. Instead an example of an important residue for the binding site, but that does not

belong to the aforementioned “key group” is E202; which if mutated into a Lys (E202K) abolishes ferrichrome binding [71], presumably because the glutamate side chain found involved in several H-bonds with backbone atoms of residues 197-199, thus determining the conformation of this essential hydroxamate-binding loop (Fig 14 and 15).

Consequently, a multiple sequence and structural-based alignment of FhuD2 with known structures of homologs, could permit predictions of ligand specificity. Sequence alignment has been performed using: BSU3320 from *B. subtilis* (PDB code: 3HXP), SirA from *S.aureus* (PDB code: 3MWG), and HtsA from *S. aureus* (PDB code: 3LHS). The alignment revealed as the best homolog, *B. subtilis* BSU3320, which maintains conserved Arg 199 (*Bs* Arg 211) and Thr112 (*Bs* Thr124), but Trp279 is functionally substituted (*Bs* Tyr295) and Trp197 is replaced by *Bs* Phe209, which lacks H-bonding capacity. However, a minor rearrangement is observed in BSU3320, where the side chain –NεH group of Trp197 is substituted by *Bs* Tyr143 donated by a neighboring loop in the C-terminal lobe. Thus, FhuD2 uses Arg, Thr and two Trp residues to bind ferrichrome, while in a slightly different but spatially equivalent manner BSU3320 presents Arg, Thr and two Tyr residues with geometries suitable for strong and specific binding to ferrichrome, or a highly similar ferric hydroxamate siderophore. Moreover, while the H-bond networks observed appear stable enough to generate specificity and affinities in the nanomolar range, they merely bind the ligand temporarily with sufficiently moderate strength to allow ligand dissociation upon fruitful engagement of the membrane receptor.

Instead, different considerations can be done on other homologs used in the alignment, where the binding architecture is totally changed: T112 is replaced by V

and S in SirA (*S.aureus*) and HtsA (*S. aureus*), respectively; W197 is replaced by a G in SirA (*S.aureus*), and S in HtsA (*S. aureus*); R199 replaced by Y and V in SirA (*S.aureus*) and HtsA (*S. aureus*), respectively; and finally, W279 is replaced by N and A in SirA (*S.aureus*) and HtsA (*S. aureus*), respectively. In conclusion, these observations confirm the specificity of binding to similar substrates (ferrichrome) by FhuD2 and BSU3320 from *B. subtilis*, and at the same time the lower sequence conservations between FhuD2 with SirA and HtsA is in agreement with their different substrates specificities, as they are both known for binding staphyloferrin, but not ferrichrome.

Making an analysis on the electrostatic residues important for FhuD2 binding, it is interesting that the basic Arg199 is in close proximity to  $Fe^{3+}$ . The positive charge on  $Fe^{3+}$  is neutralized by interaction with the ferrichrome hydroxamates [113], therefore giving to Arg199 the possibility of approaching without repulsion. The presence of a single positive residue in the binding site is common in the structures that interact with hydroxamate siderophores, differently from binding proteins having as target hydroxycarboxylate and catecholate-type siderophores, which present more positively charged side chains in their binding pockets to facilitate interaction with negatively charged ligands, such as  $Fe^{3+}$ -enterobactin that carries a -3 net charge typical of catecholate siderophores [114].

Separate discussion is done to *S.aureas* FhuD1, which shares 42% sequence identity overall and has been reported to bind hydroxamate siderophores including ferrichrome ( $K_D$  50 $\mu$ M). By previous sequence alignments, FhuD1 shows Trp197, Arg199 and Trp279 conserved, then suggesting interaction mechanisms to iron-hydroxamate very close to FhuD2. In contrast, the FhuD2 residue Thr112 is substituted by Met in FhuD1, abolishing the possibility to H-bond with the peptide



carbonyl group of ferrichrome, and this may be the molecular basis for its lower affinity. Rather than being an inferior redundant receptor for ferrichrome, FhuD1 may preferentially bind alternative currently unknown hydroxamate siderophore ligands.

Though the recognition of hydroxamate-type ferric siderophores by FhuD2 homologs appears with a similar binding model, the affinity of the ferrichrome-FhuD2 interaction is >10-fold stronger than other Binding Proteins. In fact it is reported that *E. coli* FhuD shows a  $K_D$  to Ferrichrome of 0.6-1.0 $\mu$ M [71, 115]. This difference could be attributable to *E. coli* FhuD making only three H-bonds with ferrichrome [58] , also bypassing the lack of Thr112 and Arg199 using residue Arg84, which makes multiple H-bonds with the hydroxamate groups, and no fewer than six Trp and Tyr residues which surround the siderophore [58].

These observations demonstrate how different molecular mechanisms are used by class III Binding Proteins to catch and accommodate the same siderophores targets. Particularly *E.coli* FhuD, using one less H-bond may sacrifice some affinity with the benefit that greater promiscuity may allow usage of a larger range of siderophores. This is reflected by its Arg84, which is also found able to form H-bonds with other hydroxamate siderophore as coprogen, Desferal or the antibiotic albomycin [57]. In addition, comparisons of *S. aureus* FhuD2 structure and proteins belonging to Class III have revealed two major differences: (a) the  $\alpha$ -helix that connects the two globular domains is of 25 amino acids and not of 20 (length specific for FhuD-like); (b) in FhuD2 is possible to observe the presence of more than two to three residue  $3_{10}$ -helix consistently found leading into the interdomain linker of the TroA-type PBPs: we found 6 segments of  $3_{10}$  helix of variable length, from 3 to 5, respectively.

Collectively, these differences can be involved to the highest affinity and specificity that has FhuD2 for ferrichrome, reflecting that the Gram-positive *S. aureus* acquires siderophores directly from the extracellular environment, rather than the less complex periplasmic space used by *E. coli* FhuD.

The large variety and diverse ligand specificities of the family of siderophore Binding Proteins highlights the importance of iron-acquisition in pathogenic bacteria. For example, pathogenic *N. meningitidis* has an iron acquisition system that uses a class II Binding protein (FbpA) to bind  $\text{Fe}^{3+}$  scavenged from human iron transport proteins (e.g. lactoferrin and transferrin) [116]. To address this question to *S. aureus* FhuD2, a DSF assay was used to demonstrate that ferrichrome-iron free can extract  $\text{Fe}^{3+}$  from transferrin, which thus becomes a potential source of iron for *S. aureus*, via ferrichrome. In fact transferrin alone displayed high thermal stability ( $T_m$   $80 \pm 0.6^\circ\text{C}$ ), which was greatly reduced in the presence of deferrichrome, resulting in a  $T_m$  of  $72 \pm 1.2^\circ\text{C}$ . The destabilizing effect was attributed to depletion of iron from transferrin, since iron-loaded ferrichrome had no effect on the  $T_m$  of transferrin.

Finally, we can conclude this work with two general considerations: (i) as already reported in the literature FhuD2 is able to bind siderophores not produced by *S. aureus* such as ferrichrome, aerobactin, coprogen, etc. This behavior can be described both as a competitive mechanism against bacteria that normally share with *Staphylococcus aureus* various sites of infection or a kind of cooperative mechanism always coupled to bacteria with the same infection site. (ii) The ability to use iron from transferrin through ferrichrome can assume a value of selective or cooperative mechanism on behalf to *S. aureus* extended even during the body infection. Thus, the presence of other bacteria able to synthesize ferrichrome

appears to be a requirement. These are prerequisites to describe this protein as a one of major players in two distinct phases: colonization and infection.

## References:

1. He, Y., et al., *Emerging vaccine informatics*. J Biomed Biotechnol, 2010. **2010**: p. 218590.
2. Margarit, I., et al., *Preventing bacterial infections with pilus-based vaccines: the group B streptococcus paradigm*. J Infect Dis, 2009. **199**(1): p. 108-15.
3. Giuliani, M.M., et al., *A universal vaccine for serogroup B meningococcus*. Proc Natl Acad Sci U S A, 2006. **103**(29): p. 10834-9.
4. Lucidarme, J., et al., *Characterization of fHbp, nhba (gna2132), nadA, porA, sequence type (ST), and genomic presence of IS1301 in group B meningococcal ST269 clonal complex isolates from England and Wales*. J Clin Microbiol, 2009. **47**(11): p. 3577-85.
5. Kelly, D.F. and R. Rappuoli, *Reverse vaccinology and vaccines for serogroup B Neisseria meningitidis*. Adv Exp Med Biol, 2005. **568**: p. 217-23.
6. Rinaudo, C.D., et al., *Vaccinology in the genome era*. J Clin Invest, 2009. **119**(9): p. 2515-25.
7. Rappuoli, R., *Bridging the knowledge gaps in vaccine design*. Nat Biotechnol, 2007. **25**(12): p. 1361-6.
8. Bizebard, T., et al., *Structure of influenza virus haemagglutinin complexed with a neutralizing antibody*. Nature, 1995. **376**(6535): p. 92-4.
9. Dormitzer, P.R., J.B. Ulmer, and R. Rappuoli, *Structure-based antigen design: a strategy for next generation vaccines*. Trends Biotechnol, 2008. **26**(12): p. 659-67.
10. Hewat, E.A., T.C. Marlovits, and D. Blaas, *Structure of a neutralizing antibody bound monovalently to human rhinovirus 2*. J Virol, 1998. **72**(5): p. 4396-402.
11. Harrison, S.C., *Whither structural biology?* Nat Struct Mol Biol, 2004. **11**(1): p. 12-5.
12. Kaldor, S.W., et al., *Viracept (nelfinavir mesylate, AG1343): a potent, orally bioavailable inhibitor of HIV-1 protease*. J Med Chem, 1997. **40**(24): p. 3979-85.
13. Kim, C.U., et al., *Influenza neuraminidase inhibitors possessing a novel hydrophobic interaction in the enzyme active site: design, synthesis, and structural analysis of carbocyclic sialic acid analogues with potent anti-influenza activity*. J Am Chem Soc, 1997. **119**(4): p. 681-90.
14. Joachimiak, A., *High-throughput crystallography for structural genomics*. Curr Opin Struct Biol, 2009. **19**(5): p. 573-84.
15. Bagnoli, F., et al., *Designing the next generation of vaccines for global public health*. OMICS, 2011. **15**(9): p. 545-66.
16. Abdel-Motal, U., et al., *Increased immunogenicity of human immunodeficiency virus gp120 engineered to express Galalpha1-3Galbeta1-4GlcNAc-R epitopes*. J Virol, 2006. **80**(14): p. 6943-51.
17. Godley, L., et al., *Introduction of intersubunit disulfide bonds in the membrane-distal region of the influenza hemagglutinin abolishes membrane fusion activity*. Cell, 1992. **68**(4): p. 635-45.

18. McMullan, D., et al., *High-throughput protein production for X-ray crystallography and use of size exclusion chromatography to validate or refute computational biological unit predictions*. J Struct Funct Genomics, 2005. **6**(2-3): p. 135-41.
19. Stamatos, L., M. Wiskerchen, and C. Cheng-Mayer, *Effect of major deletions in the V1 and V2 loops of a macrophage-tropic HIV type 1 isolate on viral envelope structure, cell entry, and replication*. AIDS Res Hum Retroviruses, 1998. **14**(13): p. 1129-39.
20. Cantini, F., et al., *Solution structure of the immunodominant domain of protective antigen GNA1870 of Neisseria meningitidis*. J Biol Chem, 2006. **281**(11): p. 7220-7.
21. Scarselli, M., et al., *Rational design of a meningococcal antigen inducing broad protective immunity*. Sci Transl Med, 2011. **3**(91): p. 91ra62.
22. Foster, T., *Staphylococcus*. 1996.
23. Chesney, P.J., *Toxic-shock syndrome: a commentary and review of the characteristics of Staphylococcus aureus strains*. Infection, 1983. **11**(4): p. 181-8.
24. Christensen, G.D., et al., *Characterization of clinically significant strains of coagulase-negative staphylococci*. J Clin Microbiol, 1983. **18**(2): p. 258-69.
25. Baron, D.N. and P.M. Fraser, *Medical applications of taxonomic methods*. Br Med Bull, 1968. **24**(3): p. 236-40.
26. Klein, E., D.L. Smith, and R. Laxminarayan, *Hospitalizations and deaths caused by methicillin-resistant Staphylococcus aureus, United States, 1999-2005*. Emerg Infect Dis, 2007. **13**(12): p. 1840-6.
27. Klein, E., D.L. Smith, and R. Laxminarayan, *Community-associated methicillin-resistant Staphylococcus aureus in outpatients, United States, 1999-2006*. Emerg Infect Dis, 2009. **15**(12): p. 1925-30.
28. Ganz, T. and E. Nemeth, *Regulation of iron acquisition and iron distribution in mammals*. Biochim Biophys Acta, 2006. **1763**(7): p. 690-9.
29. Le, N.T. and D.R. Richardson, *The role of iron in cell cycle progression and the proliferation of neoplastic cells*. Biochim Biophys Acta, 2002. **1603**(1): p. 31-46.
30. Lukianova, O.A. and S.S. David, *A role for iron-sulfur clusters in DNA repair*. Curr Opin Chem Biol, 2005. **9**(2): p. 145-51.
31. Kochan, I., *The role of iron in bacterial infections, with special consideration of host-tubercle bacillus interaction*. Curr Top Microbiol Immunol, 1973. **60**: p. 1-30.
32. Weinberg, E.D., *Iron availability and infection*. Biochim Biophys Acta, 2009. **1790**(7): p. 600-5.
33. Braun, V., K. Hantke, and W. Koster, *Bacterial iron transport: mechanisms, genetics, and regulation*. Met Ions Biol Syst, 1998. **35**: p. 67-145.
34. Cassat, J.E. and E.P. Skaar, *Metal ion acquisition in Staphylococcus aureus: overcoming nutritional immunity*. Semin Immunopathol, 2012. **34**(2): p. 215-35.
35. Beasley, F.C., et al., *Characterization of staphyloferrin A biosynthetic and transport mutants in Staphylococcus aureus*. Mol Microbiol, 2009. **72**(4): p. 947-63.
36. Cotton, J.L., J. Tao, and C.J. Balibar, *Identification and characterization of the Staphylococcus aureus gene cluster coding for staphyloferrin A*. Biochemistry, 2009. **48**(5): p. 1025-35.
37. Cheung, J., et al., *Molecular characterization of staphyloferrin B biosynthesis in Staphylococcus aureus*. Mol Microbiol, 2009. **74**(3): p. 594-608.

38. Friedman, D.B., et al., *Staphylococcus aureus* redirects central metabolism to increase iron availability. PLoS Pathog, 2006. **2**(8): p. e87.
39. Horsburgh, M.J., E. Ingham, and S.J. Foster, *In Staphylococcus aureus, fur is an interactive regulator with PerR, contributes to virulence, and is necessary for oxidative stress resistance through positive regulation of catalase and iron homeostasis.* J Bacteriol, 2001. **183**(2): p. 468-75.
40. Hantke, K., *Regulation of ferric iron transport in Escherichia coli K12: isolation of a constitutive mutant.* Mol Gen Genet, 1981. **182**(2): p. 288-92.
41. Xiong, A., et al., *Molecular characterization of the ferric-uptake regulator, fur, from Staphylococcus aureus.* Microbiology, 2000. **146 ( Pt 3)**: p. 659-68.
42. Skaar, E.P. and O. Schneewind, *Iron-regulated surface determinants (Isd) of Staphylococcus aureus: stealing iron from heme.* Microbes Infect, 2004. **6**(4): p. 390-7.
43. Mazmanian, S.K., et al., *Passage of heme-iron across the envelope of Staphylococcus aureus.* Science, 2003. **299**(5608): p. 906-9.
44. Sharp, K.H., et al., *Crystal structure of the heme-IsdC complex, the central conduit of the Isd iron/heme uptake system in Staphylococcus aureus.* J Biol Chem, 2007. **282**(14): p. 10625-31.
45. Hammer, N.D. and E.P. Skaar, *Molecular mechanisms of Staphylococcus aureus iron acquisition.* Annu Rev Microbiol, 2011. **65**: p. 129-47.
46. Dale, S.E., et al., *Role of siderophore biosynthesis in virulence of Staphylococcus aureus: identification and characterization of genes involved in production of a siderophore.* Infect Immun, 2004. **72**(1): p. 29-37.
47. Sebulsky, M.T., et al., *FhuD1, a ferric hydroxamate-binding lipoprotein in Staphylococcus aureus: a case of gene duplication and lateral transfer.* J Biol Chem, 2004. **279**(51): p. 53152-9.
48. Speziali, C.D., et al., *Requirement of Staphylococcus aureus ATP-binding cassette-ATPase FhuC for iron-restricted growth and evidence that it functions with more than one iron transporter.* J Bacteriol, 2006. **188**(6): p. 2048-55.
49. Guerout-Fleury, A.M., et al., *Antibiotic-resistance cassettes for Bacillus subtilis.* Gene, 1995. **167**(1-2): p. 335-6.
50. Chu, B.C. and H.J. Vogel, *A structural and functional analysis of type III periplasmic and substrate binding proteins: their role in bacterial siderophore and heme transport.* Biol Chem, 2011. **392**(1-2): p. 39-52.
51. Quijcho, F.A. and P.S. Ledvina, *Atomic structure and specificity of bacterial periplasmic receptors for active transport and chemotaxis: variation of common themes.* Mol Microbiol, 1996. **20**(1): p. 17-25.
52. Krewulak, K.D., R.S. Peacock, and H.J. Vogel, *Periplasmic binding proteins involved in bacterial iron uptake,* in *Iron Transport in Bacteria*, J.H. Crosa, A.R. Mey, and S.M. Payne, Editors. 2004, ASM Press: Washington, DC. p. 113-29.
53. Mao, B., et al., *Hinge-bending in L-arabinose-binding protein. The "Venus's-flytrap" model.* J Biol Chem, 1982. **257**(3): p. 1131-3.
54. Sharff, A.J., et al., *Crystallographic evidence of a large ligand-induced hinge-twist motion between the two domains of the maltodextrin binding protein involved in active transport and chemotaxis.* Biochemistry, 1992. **31**(44): p. 10657-63.
55. Spurlino, J.C., G.Y. Lu, and F.A. Quijcho, *The 2.3-A resolution structure of the maltose- or maltodextrin-binding protein, a primary receptor of bacterial active transport and chemotaxis.* J Biol Chem, 1991. **266**(8): p. 5202-19.

56. Sack, J.S., M.A. Saper, and F.A. Quioco, *Periplasmic binding protein structure and function. Refined X-ray structures of the leucine/isoleucine/valine-binding protein and its complex with leucine.* J Mol Biol, 1989. **206**(1): p. 171-91.
57. Clarke, T.E., et al., *X-ray crystallographic structures of the Escherichia coli periplasmic protein FhuD bound to hydroxamate-type siderophores and the antibiotic albomycin.* J Biol Chem, 2002. **277**(16): p. 13966-72.
58. Clarke, T.E., et al., *The structure of the ferric siderophore binding protein FhuD complexed with gallichrome.* Nat Struct Biol, 2000. **7**(4): p. 287-91.
59. Krewulak, K.D., C.M. Shepherd, and H.J. Vogel, *Molecular dynamics simulations of the periplasmic ferric-hydroxamate binding protein FhuD.* Biometals, 2005. **18**(4): p. 375-86.
60. Borths, E.L., et al., *The structure of Escherichia coli BtuF and binding to its cognate ATP binding cassette transporter.* Proc Natl Acad Sci U S A, 2002. **99**(26): p. 16642-7.
61. Krewulak, K.D. and H.J. Vogel, *Structural biology of bacterial iron uptake.* Biochim Biophys Acta, 2008. **1778**(9): p. 1781-804.
62. Ma, Z., F.E. Jacobsen, and D.P. Giedroc, *Coordination chemistry of bacterial metal transport and sensing.* Chem Rev, 2009. **109**(10): p. 4644-81.
63. Skaar, E.P., et al., *Iron-source preference of Staphylococcus aureus infections.* Science, 2004. **305**(5690): p. 1626-8.
64. Wandersman, C. and P. Delepelaire, *Bacterial iron sources: from siderophores to hemophores.* Annu Rev Microbiol, 2004. **58**: p. 611-47.
65. Sebulsky, M.T. and D.E. Heinrichs, *Identification and characterization of fhuD1 and fhuD2, two genes involved in iron-hydroxamate uptake in Staphylococcus aureus.* J Bacteriol, 2001. **183**(17): p. 4994-5000.
66. Heinrichs, J.H., et al., *Identification and characterization of SirA, an iron-regulated protein from Staphylococcus aureus.* J Bacteriol, 1999. **181**(5): p. 1436-43.
67. Konetschny-Rapp, S., et al., *Staphyloferrin A: a structurally new siderophore from staphylococci.* Eur J Biochem, 1990. **191**(1): p. 65-74.
68. Sebulsky, M.T., et al., *Identification and characterization of a membrane permease involved in iron-hydroxamate transport in Staphylococcus aureus.* J Bacteriol, 2000. **182**(16): p. 4394-400.
69. Chu, B.C., et al., *Siderophore uptake in bacteria and the battle for iron with the host; a bird's eye view.* Biometals, 2010. **23**(4): p. 601-11.
70. Grigg, J.C., et al., *The Staphylococcus aureus siderophore receptor HtsA undergoes localized conformational changes to enclose staphyloferrin A in an arginine-rich binding pocket.* J Biol Chem, 2010. **285**(15): p. 11162-71.
71. Sebulsky, M.T., et al., *The role of FhuD2 in iron(III)-hydroxamate transport in Staphylococcus aureus. Demonstration that FhuD2 binds iron(III)-hydroxamates but with minimal conformational change and implication of mutations on transport.* J Biol Chem, 2003. **278**(50): p. 49890-900.
72. Greenfield, N.J., *Using circular dichroism spectra to estimate protein secondary structure.* Nat Protoc, 2006. **1**(6): p. 2876-90.
73. Greenfield, N.J., *Using circular dichroism collected as a function of temperature to determine the thermodynamics of protein unfolding and binding interactions.* Nat Protoc, 2006. **1**(6): p. 2527-35.
74. Kelly, S.M. and N.C. Price, *The use of circular dichroism in the investigation of protein structure and function.* Curr Protein Pept Sci, 2000. **1**(4): p. 349-84.

75. Niesen, F.H., H. Berglund, and M. Vedadi, *The use of differential scanning fluorimetry to detect ligand interactions that promote protein stability*. Nat Protoc, 2007. **2**(9): p. 2212-21.
76. Goldberg, D.S., et al., *Formulation development of therapeutic monoclonal antibodies using high-throughput fluorescence and static light scattering techniques: Role of conformational and colloidal stability*. J Pharm Sci, 2010.
77. Vedadi, M., et al., *Chemical screening methods to identify ligands that promote protein stability, protein crystallization, and structure determination*. Proc Natl Acad Sci U S A, 2006. **103**(43): p. 15835-40.
78. Murphy, M., L. Jason-Moller, and J. Bruno, *Using Biacore to measure the binding kinetics of an antibody-antigen interaction*. Curr Protoc Protein Sci, 2006. **Chapter 19**: p. Unit 19 14.
79. Jason-Moller, L., M. Murphy, and J. Bruno, *Overview of Biacore systems and their applications*. Curr Protoc Protein Sci, 2006. **Chapter 19**: p. Unit 19 13.
80. Otwinowski, Z. and W. Minor, *Processing of X-ray Diffraction Data Collected in Oscillation Mode*. Methods Enzymol, 1997. **276**: p. 307-26.
81. CCP4, *The CCP4 suite: programs for protein crystallography*. Acta Crystallogr D Biol Crystallogr, 1994. **50**(Pt 5): p. 760-3.
82. McCoy, A.J., et al., *Phaser crystallographic software*. J Appl Crystallogr, 2007. **40**(Pt 4): p. 658-674.
83. Adams, P.D., et al., *PHENIX: a comprehensive Python-based system for macromolecular structure solution*. Acta Crystallogr D Biol Crystallogr, 2010. **66**(Pt 2): p. 213-21.
84. Emsley, P. and K. Cowtan, *Coot: model-building tools for molecular graphics*. Acta Crystallogr D Biol Crystallogr, 2004. **60**(Pt 12 Pt 1): p. 2126-32.
85. Davis, I.W., et al., *MOLPROBITY: structure validation and all-atom contact analysis for nucleic acids and their complexes*. Nucleic Acids Res, 2004. **32**(Web Server issue): p. W615-9.
86. Matthews, B.W., *Solvent content of protein crystals*. J Mol Biol, 1968. **33**(2): p. 491-7.
87. Chan, A.W., et al., *Identification, classification, and analysis of beta-bulges in proteins*. Protein Sci, 1993. **2**(10): p. 1574-90.
88. Lewis, P.N., F.A. Momany, and H.A. Scheraga, *Folding of polypeptide chains in proteins: a proposed mechanism for folding*. Proc Natl Acad Sci U S A, 1971. **68**(9): p. 2293-7.
89. Lewis, P.N., F.A. Momany, and H.A. Scheraga, *Chain reversals in proteins*. Biochim Biophys Acta, 1973. **303**(2): p. 211-29.
90. Kuntz, I.D., *Protein folding*. J Am Chem Soc, 1972. **94**(11): p. 4009-12.
91. Crawford, J.L., W.N. Lipscomb, and C.G. Schellman, *The reverse turn as a polypeptide conformation in globular proteins*. Proc Natl Acad Sci U S A, 1973. **70**(2): p. 538-42.
92. Chou, P.Y. and G.D. Fasman, *Prediction of protein conformation*. Biochemistry, 1974. **13**(2): p. 222-45.
93. Rao, S.T. and M.G. Rossmann, *Comparison of super-secondary structures in proteins*. J Mol Biol, 1973. **76**(2): p. 241-56.
94. Yuan, Z., T.L. Bailey, and R.D. Teasdale, *Prediction of protein B-factor profiles*. Proteins, 2005. **58**(4): p. 905-12.
95. Grigg, J.C., et al., *Specificity of Staphyloferrin B recognition by the SirA receptor from Staphylococcus aureus*. J Biol Chem, 2010. **285**(45): p. 34579-88.



96. Shi, R., et al., *Trapping open and closed forms of FitE: a group III periplasmic binding protein*. Proteins, 2009. **75**(3): p. 598-609.
97. Peuckert, F., et al., *The siderophore binding protein FeuA shows limited promiscuity toward exogenous triscatecholates*. Chem Biol, 2011. **18**(7): p. 907-19.
98. Finch, C.A. and H.A. Huebers, *Maintenance of normal iron balance*. Haematologia (Budap), 1987. **20**(4): p. 225-8.
99. Ponka, P. and D.R. Richardson, *Can ferritin provide iron for hemoglobin synthesis?* Blood, 1997. **89**(7): p. 2611-3.
100. Ponka, P., *Tissue-specific regulation of iron metabolism and heme synthesis: distinct control mechanisms in erythroid cells*. Blood, 1997. **89**(1): p. 1-25.
101. Tsagalis, G., *Renal anemia: a nephrologist's view*. Hippokratia, 2011. **15**(Suppl 1): p. 39-43.
102. Huebers, H.A. and C.A. Finch, *Transferrin: physiologic behavior and clinical implications*. Blood, 1984. **64**(4): p. 763-7.
103. Wink, D.A., et al., *Reaction kinetics for nitrosation of cysteine and glutathione in aerobic nitric oxide solutions at neutral pH. Insights into the fate and physiological effects of intermediates generated in the NO/O<sub>2</sub> reaction*. Chem Res Toxicol, 1994. **7**(4): p. 519-25.
104. Walling, C., R.E. Partch, and T. Weil, *Kinetics of the decomposition of hydrogen peroxide catalyzed by ferric ethylenediaminetetraacetate complex*. Proc Natl Acad Sci U S A, 1975. **72**(1): p. 140-2.
105. Rahman, K., *Studies on free radicals, antioxidants, and co-factors*. Clin Interv Aging, 2007. **2**(2): p. 219-36.
106. Miethke, M., S. Schmidt, and M.A. Marahiel, *The major facilitator superfamily-type transporter YmfE and the multidrug-efflux activator Mta mediate bacillibactin secretion in Bacillus subtilis*. J Bacteriol, 2008. **190**(15): p. 5143-52.
107. Fukami-Kobayashi, K., Y. Tateno, and K. Nishikawa, *Domain dislocation: a change of core structure in periplasmic binding proteins in their evolutionary history*. J Mol Biol, 1999. **286**(1): p. 279-90.
108. Tam, R. and M.H. Saier, Jr., *Structural, functional, and evolutionary relationships among extracellular solute-binding receptors of bacteria*. Microbiol Rev, 1993. **57**(2): p. 320-46.
109. Claverys, J.P., *A new family of high-affinity ABC manganese and zinc permeases*. Res Microbiol, 2001. **152**(3-4): p. 231-43.
110. Lee, Y.H., et al., *The crystal structure of Zn(II)-free Treponema pallidum TroA, a periplasmic metal-binding protein, reveals a closed conformation*. J Bacteriol, 2002. **184**(8): p. 2300-4.
111. Lee, Y.H., et al., *Treponema pallidum TroA is a periplasmic zinc-binding protein with a helical backbone*. Nat Struct Biol, 1999. **6**(7): p. 628-33.
112. Oke, M., et al., *The Scottish Structural Proteomics Facility: targets, methods and outputs*. J Struct Funct Genomics, 2010. **11**(2): p. 167-80.
113. Winkelmann, G., *Ecology of siderophores with special reference to the fungi*. Biometals, 2007. **20**(3-4): p. 379-92.
114. Karpishin, T.B., T.D.P. Stack, and K.N. Raymond, *Stereoselectivity in Chiral Fe(III) and Ga(III) Tris(Catecholate) Complexes Effected by Nonbonded, Weakly Polar Interactions*. Journal of the American Chemical Society, 1993. **115**(14): p. 6115-6125.
115. Rohrbach, M.R., V. Braun, and W. Koster, *Ferrichrome transport in Escherichia coli K-12: altered substrate specificity of mutated periplasmic FhuD and interaction of FhuD with the integral membrane protein FhuB*. J Bacteriol, 1995. **177**(24): p. 7186-93.

116. Perkins-Balding, D., M. Ratliff-Griffin, and I. Stojilkovic, *Iron transport systems in Neisseria meningitidis*. Microbiol Mol Biol Rev, 2004. **68**(1): p. 154-71.